Quantifying inclination shallowing and representing flattening uncertainty in sedimentary paleomagnetic poles

James Pierce[1], Yiming Zhang[2], Eben Hodgin[3], and Nicholas L Swanson-Hysell[2]

[1]Yale University
[2]University of California, Berkeley
[3]University of California

November 24, 2022

Abstract

Inclination is the angle of a magnetization vector from horizontal. Clastic sedimentary rocks often experience inclination shallowing whereby syn- to post-depositional processes result in flattened detrital remanent magnetizations relative to local geomagnetic field inclinations. The deviation of recorded inclinations from the true values presents challenges for reconstructing paleolatitudes. A widespread approach for estimating the flattening factor (f) compares the shape of an assemblage of magnetization vectors to that derived from a paleosecular variation model (the elongation/inclination [E/I] method). However, few studies exist that compare the results of this statistical approach with empirically determined flattening factors and none in the Proterozoic Eon. In this study, we evaluate inclination shallowing within 1.1 billion-year-old, hematite-bearing, interflow red beds of the Cut Face Creek Sandstone that is bounded by lava flows of known inclination. We found that detrital hematite remanence is flattened with f = 0.65{0.75}_{0.56}$ whereas the pigmentary hematite magnetization shares a common mean with the volcanics. Comparison of detrital and pigmentary hematite directions results in $f = 0.61^{0.67}_{0.55}$. These empirically determined flattening factors are consistent with those estimated through the E/I method ($f = 0.64^{0.85}_{0.51}$) supporting its application in deep time. However, all methods have significant uncertainty associated with determining the flattening factor. This uncertainty can be incorporated into the calculation of paleomagnetic poles with the resulting ellipse approximated with a Kent distribution. Rather than seeking to find "the flattening factor,' or assuming a single value, the inherent uncertainty in flattening factors should be recognized and incorporated into paleomagnetic syntheses.

Quantifying inclination shallowing and representing flattening uncertainty in sedimentary paleomagnetic poles

James Pierce[1,2], **Yiming Zhang**[1], **Eben B. Hodgin**[1], **Nicholas L. Swanson-Hysell**[1]

[1]Department of Earth and Planetary Science, University of California, Berkeley, CA, USA
[2]Department of Earth and Planetary Sciences, Yale University, New Haven, CT, USA

Key Points:

- Inclination shallowing is empirically quantified in 1.1 Ga clastic sedimentary rocks bracketed by volcanics
- Detrital hematite remanence is flattened by a factor of $0.61^{0.67}_{0.55}$ relative to unflattened pigmentary hematite
- Flattening factor uncertainty is present in all methods and should be incorporated into the uncertainty of sedimentary paleomagnetic poles

Corresponding author: James Pierce (james.pierce@yale.edu); Nicholas Swanson-Hysell (swanson-hysell@berkeley.edu),

Abstract

Inclination is the angle of a magnetization vector from horizontal. Clastic sedimentary rocks often experience inclination shallowing whereby syn- to post-depositional processes result in flattened detrital remanent magnetizations relative to local geomagnetic field inclinations. The deviation of recorded inclinations from the true values presents challenges for reconstructing paleolatitudes. A widespread approach for estimating the flattening factor (f) compares the shape of an assemblage of magnetization vectors to that derived from a paleosecular variation model (the elongation/inclination [E/I] method). However, few studies exist that compare the results of this statistical approach with empirically determined flattening factors and none in the Proterozoic Eon. In this study, we evaluate inclination shallowing within 1.1 billion-year-old, hematite-bearing, interflow red beds of the Cut Face Creek Sandstone that is bounded by lava flows of known inclination. We found that detrital hematite remanence is flattened with $f = 0.65^{0.75}_{0.56}$ whereas the pigmentary hematite magnetization shares a common mean with the volcanics. Comparison of detrital and pigmentary hematite directions results in $f = 0.61^{0.67}_{0.55}$. These empirically determined flattening factors are consistent with those estimated through the E/I method ($f = 0.64^{0.85}_{0.51}$) supporting its application in deep time. However, all methods have significant uncertainty associated with determining the flattening factor. This uncertainty can be incorporated into the calculation of paleomagnetic poles with the resulting ellipse approximated with a Kent distribution. Rather than seeking to find "the flattening factor," or assuming a single value, the inherent uncertainty in flattening factors should be recognized and incorporated into paleomagnetic syntheses.

Plain Language Summary

The magnetization of ancient sedimentary rocks provides great insight into Earth's past. Earth scientists use these rocks to understand how Earth's magnetic field has flipped through time and to reconstruct how continents have moved. Hematite is a common mineral which gives many sandstones a red color — leading geologists to refer to them as "red beds." While hematite is a reliable magnet through time, the magnetic directions recorded by hematite grains can be shallower than the geomagnetic field (i.e. they are flattened). Magnetization steepness is how Earth scientists determine the latitude where rocks were deposited as the magnetic field gets steeper towards the pole. We need ways to correct for magnetization shallowing in sedimentary rocks. In this study, we compared the steepness of magnetic directions held by hematite to that of lava flows that formed in the same time interval. Magnetic directions from lava flows are not flattened so this comparison allows us to determine the shallowing amount. We compare it to a statistical method and see that the results are indistinguishable within the appreciable uncertainty of the methods. Earth scientists should include the uncertainty associated with inclination shallowing when they report ancient pole positions determined from such flattened magnetic directions.

1 Introduction

Hematite-bearing sedimentary rocks at Earth's surface are widespread and serve as an important paleomagnetic recorder. The geocentric axial dipole (GAD) hypothesis posits that the long-term average of Earth's magnetic field is dipolar and that the time-averaged geomagnetic pole overlaps with the geographic pole. Using this hypothesis, the inclination (I) of a rock's magnetization can be translated into an interpreted paleolatitude (ϕ) of the location where the rock formed using the dipole formula:

$$\tan(I) = 2\tan(\phi)$$

Unfortunately, the accuracy of paleomagnetic directions recorded by the detrital remanent magnetization (DRM) of sedimentary rocks has long been recognized as problematic due to the issue of inclination shallowing (King, 1955; Tauxe & Kent, 1984; Kodama, 2012). The rotation of ferromagnetic grains during deposition and compaction can result in the acquisition of a detrital remanent magnetization that is biased shallow relative to the local geomagnetic field in which it was acquired (Tauxe, 2005). If uncorrected, shallower inclinations obtained from sedimentary rocks can potentially result in erroneously low estimates of paleolatitudes, biasing the interpreted past positions of continents and hindering plate reconstructions (Domeier et al., 2012). Despite this challenge, the abundance and long-term magnetic and geochemical stability of hematite makes hematite-bearing sedimentary rocks a very important archive of Earth history.

In addition to detrital hematite grains that can carry a DRM, hematite-bearing sedimentary rocks often have a distinct population of pigmentary hematite that give "red beds" their characteristic red color. This finer-grained pigmentary hematite precipitates following deposition and carries a chemical remanent magnetization (CRM) acquired during crystal growth (Tauxe et al., 1980; Jiang et al., 2015; Swanson-Hysell et al., 2019).

This pigmentary hematite can form from metastable Fe(III) oxide precursors such as ferrihydrite (Gutiérrez et al., 2016; Jiang et al., 2018, 2022). Such pigmentary hematite records a magnetization when it grows to be the size of a stable single domain particle (~30 nm; Özdemir and Dunlop (2014)). Although the CRMs acquired by pigmentary hematite are not expected to be shallowed, the time lag between sediment deposition and secondary pigmentary hematite formation can be variable which complicates interpretations. Fortunately, magnetization held by primary detrital hematite can be isolated from that held by finer-grained secondary pigmentary hematite through high resolution thermal demagnetization as hematite grains less than ~400 nm in diameter will unblock at lower temperatures than coarser detrital grains (Tauxe et al., 1980; Swanson-Hysell et al., 2019). After thermal demagnetization of pigmentary hematite, the DRM held by coarser hematite grains will become apparent near hematite's Néel Temperature (~682°C; Butler (1992); Lu and Meng (2010)).

To elucidate factors that contribute to inclination shallowing of detrital magnetization in sedimentary rocks, King (1955) conducted laboratory redeposition experiments and quantified the shallowing effect with the flattening function:

$$\tan(I_o) = f \tan(I_f)$$

where I_o represents the observed inclination of the specimen magnetization and I_f represents the inclination of the field in which the magnetization was acquired (Fig. 1). The flattening factor f ranges from 1 for no flattening to 0 for completely flattened inclinations (Fig. 1). Further laboratory redeposition experiments have found that major contributing processes to inclination shallowing include the initial settling and deposition of particles as well as compaction during burial (Anson & Kodama, 1987; Tauxe & Kent, 1984; Sun & Kodama, 1992; Tan et al., 2002). The degree of flattening can also be influenced by sedimentary lithology with finer grained sediments exhibiting more inclination shallowing in laboratory experiments (Tan et al., 2002).

Correcting the effects of inclination shallowing is crucial for estimating the inclination of the geomagnetic field at the time of deposition. Two main classes of correction methods have been developed and applied in order to determine and correct for inclination shallowing. The first class of methods involves investigating the magnetic fabrics of the sedimentary rocks of interest. Such an approach was pioneered by Jackson et al. (1991), where anisotropy of anhysteretic magnetization (AARM) was used to es-

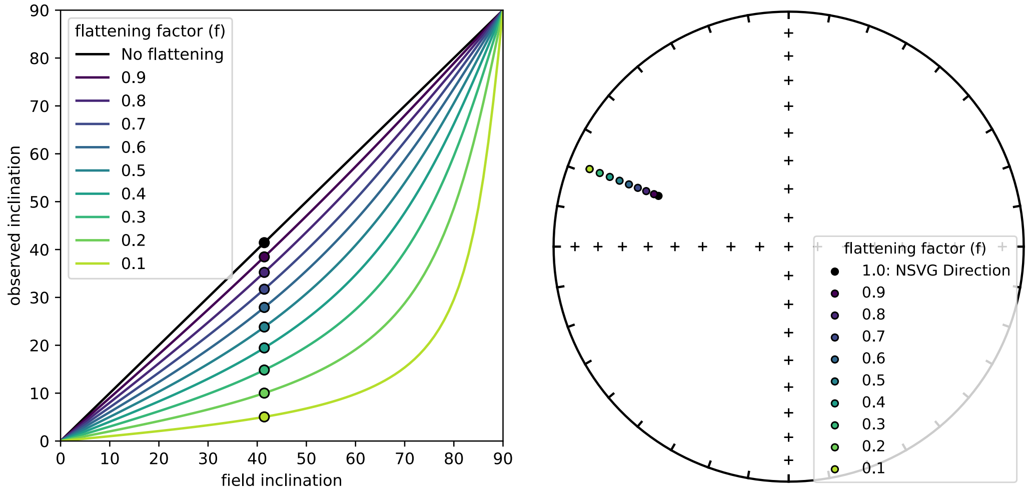

Figure 1: Left panel: the relationship between the inclination of the local magnetic field compared to the observed inclination of sedimentary rocks is shown for different flattening factors (f). A value of 1.0 corresponds to no flattening while a value of 0.0 means the magnetizations are completely flattened. The dots show the inclination expected for the Cut Face Creek Sandstone that would result from variable flattening of the mean inclination of lavas from the upper northeast sequence of the North Shore Volcanic Group (NSVG; Tauxe and Kodama (2009); Swanson-Hysell et al. (2019)). Right panel: an equal area plot with the mean paleomagnetic direction of the upper northeast sequence North Shore Volcanic Group lavas (declination of 290.7°; inclination of 41.4°) and the directions that would result from applying different flattening factors.

timate and correct shallowed inclinations. Subsequent work has highlighted the importance of determining the relationship between shallowing and magnetic anisotropy associated with a given sedimentary rock in the application of the method (Kodama, 2012). A particular difficulty in applying this method to correct detrital remanent magnetizations in hematite-bearing sedimentary rocks is that both pigmentary hematite and detrital hematite contribute to the overall magnetic fabric with the anisotropy associated with the detrital population needing to be isolated for an inclination shallowing correction. Recognizing this challenge, Bilardello (2015) developed a more involved multispecimen approach using step-wise thermal demagnetization of applied isothermal remanent magnetizations (IRM) in order to isolate the anisotropy of DRM. Overall, such anisotropy approaches are labor-intensive and have only been applied to quantify inclination shallowing in a modest number of studies.

The other principal method for correcting inclination shallowing is the statistical elongation/inclination (E/I) approach (Tauxe & Kent, 2004). This method utilizes the fact that inclination shallowing will skew the shape of the population of recorded magnetization vectors away from a distribution expected from secular variation of Earth's magnetic field. The E/I method uses the TK03 model for paleosecular variation which is based on a compilation of paleomagnetic directions from lava flows of the last 5 million years (McElhinny & McFadden, 1997) to predict the original distribution and shape of paleomagnetic directions based on a Giant Gaussian Process approach. In this model, the distribution of paleomagnetic directions at a given latitude that sufficiently samples paleosecular variation has a predictable elongated shape that deviates from circular symmetry as a function of inclination. The shape of the distribution of vectors is quantified by the elongation parameter (E) that can be determined by calculating the eigenvalue ratio τ_2/τ_3 of the orientation matrix for a population of vectors. One can estimate the amount of inclination shallowing in a sedimentary rock by progressively unflattening the shallowed magnetization vectors until their distribution best matches the predicted shape. This approach assumes that the TK03.GAD model accurately characterizes the paleosecular variation during acquisition of magnetization in the sedimentary formation of interest. The uncertainty on the flattening factor that leads to a correspondence between the elongation of the magnetization vectors with the E/I of the TK03.GAD model can be estimated through bootstrap resampling (Tauxe & Kent, 2004). As a statistical method, the E/I has the benefit that the analyses are done on specimen DRM magnetization directions and it does not require additional labor-intensive anisotropy measurements which includes the necessary determination of individual particle anisotropy. However, this method requires a large number of DRM directions (>100) as many more vectors are needed to accurately determine the shape of a distribution than the mean of a distribution (Tauxe et al., 2008). The large number of directions needed to reliably apply the method led Vaes et al. (2021) to propose a classification scheme wherein >100 directions are needed for a corrected sedimentary pole to be deemed reliable (as well as paleosecular variation being assessed using the criteria of Deenen et al. (2011)).

Due to the challenges of applying these inclination correction methods, particularly to previously published data, another simplified approach that has been taken in the literature is to assume an average f factor and apply it to the mean direction calculated from a sedimentary rock (Domeier et al., 2012; Torsvik et al., 2012). For many published data sets from sedimentary rocks where the specimen level data are not available and compilations are reliant on study level means, such an approach is the only one that can be applied without redoing the study. This approach was applied by Torsvik et al. (2012)

in their compilation of Phanerozoic paleomagnetic poles where a flattening factor of 0.6 was used to correct sedimentary poles. Domeier et al. (2012) also adopted a flattening factor of 0.6 acknowledging that to do so is an oversimplification, but a value that is consistent with compiled f factor estimates (such as those of Bilardello and Kodama (2010c)). This approach has been criticized as disregarding the variability of f factors that can result from differences in lithology and magnetic carriers (Bilardello, 2016; Vaes et al., 2021). There have been other novel data analysis approaches to seek to constrain f factors such as through comparing intersecting great circles from multiple paleomagnetic poles in the true dipole pole method of Gallo et al. (2017). For any method, there is a challenge of applying a single f factor to a sedimentary formation given variability associated with grain size and other conditions.

In this study, we use the ca. 1093 Ma Cut Face Creek Sandstone to empirically constrain the magnitude of inclination shallowing. The Cut Face Creek Sandstone is a ∼95 meter-thick interval of interflow red siltstone and sandstone deposited in a fluvial overbank depositional environment between lava flows of the upper northeast sequence of the North Shore Volcanic Group (Fig. 2). Since the sandstone is bracketed by lava flows with known age and existing paleomagnetic data, its age and expected paleomagnetic direction is well constrained (Tauxe & Kodama, 2009; Swanson-Hysell et al., 2019). We compare the detrital remanence directions of the Cut Face Creek specimens to the expected directions from the volcanics to determine the amount of inclination shallowing that took place within the sedimentary unit. Next, we apply the elongation/inclination method to the isolated DRM directions to obtain statistical estimates for the amount of shallowing that can be compared to the empirically determined value. Finally, we present recommendations for the incorporation of uncertainties in flattening factor estimates into sedimentary paleomagnetic poles and paleolatitude estimates as such uncertainties are present regardless of the method through which they are determined.

2 Geologic Setting and stratigraphy of the Cut Face Creek Sandstone

The Mesoproterozoic Midcontinent Rift is a protracted intracontinental rift punctuated by rapid and voluminous magmatism throughout its history (Fig. 2A; Green (1983); Swanson-Hysell et al. (2021)). A ∼8 km thick succession of lava flows that erupted during Midcontinent Rift development is exposed in northeastern Minnesota forming the northeast sequence of the North Shore Volcanic Group (Fig. 2B; Green et al. (2011)).

Our study is focused on the ~95-meter-thick Cut Face Creek Sandstone which is an interflow fluvial siliciclastic unit that was deposited during a hiatus in lava flow eruptions (Jirsa, 1984). It is bracketed by the underlying Good Harbor Bay andesites and the overlying Terrace Point Basalt (Figs. 2C and 3). These units are all part of the normal-polarity upper northeast sequence of the North Shore Volcanic Group (Figs. 2; Green et al. (2011)). The Grand Marais Rhyolite with a high-precision weighted mean ^{206}Pb/^{238}U zircon date of 1093.52 ± 0.43 Ma (Swanson-Hysell et al., 2019) is ~250 m stratigraphically below the Good Harbor Bay andesites (Green et al., 2011). Its age serves as a maximum age constraint for the deposition of Cut Face Creek Sandstone and is likely close to the absolute age. The minimum depositional age of the sandstone is constrained by the 1091.7 ± 0.2 Ma Beaver River diabase of the Beaver Bay Complex, which crosscuts the North Shore Volcanic Group (Zhang et al., 2021). Paleomagnetic data from twenty-eight lava flows of the upper Northeast sequence of the North Shore Volcanic Group (blue diamonds in Fig. 2; Books (1972); Tauxe and Kodama (2009)) result in a paleomagnetic pole at 181.7°E, 31.1°N (A_{95}=4.2°; Swanson-Hysell et al. (2019)). This pole from the volcanics can be used to calculate an expected paleomagnetic direction for the Cut Face Creek Sandstone with a declination of 290.7° and an inclination of 41.4° (Fig. 1).

The Cut Face Creek Sandstone is well-exposed in a prominent roadcut along Minnesota State Highway 61 with a striking deep red color (47.7280°N, 90.4428°W; Figs. 2 and 3). Throughout the section, the strata are consistently tilted to the southeast with an average dip direction of 166.5° and dip of 10.0° (based on 44 measurements). Our stratigraphic section through the ~95-meter-thick Cut Face Creek Sandstone was measured at a decimeter scale upward from its base where it overlies the uppermost lava flow of the Good Harbor Bay andesites (Fig. 3).

The Good Harbor Bay andesites are fine-grained, greenish-grey, volcanic rocks that become increasingly vesicular toward flow tops. In the measured stratigraphic section, the uppermost lava is overlain by a 0.9-meter-thick silt-sized matrix-supported basalt pebble conglomerate with sand lenses and mud cracks (Fig. 3). This conglomerate is followed by ~17.5 m of medium to fine-grained lithic arkose that generally fines upwards. The medium-grained sandstone is associated with occasional decimeter-scale dune-scale trough cross-bedding characteristic of channel bars. Finer-grained sandstone beds that contain regular mm-scale siltstone laminae, mudcracks, and current ripples with variable flow directions, are characteristic of crevasse splay deposits which occur when a stream

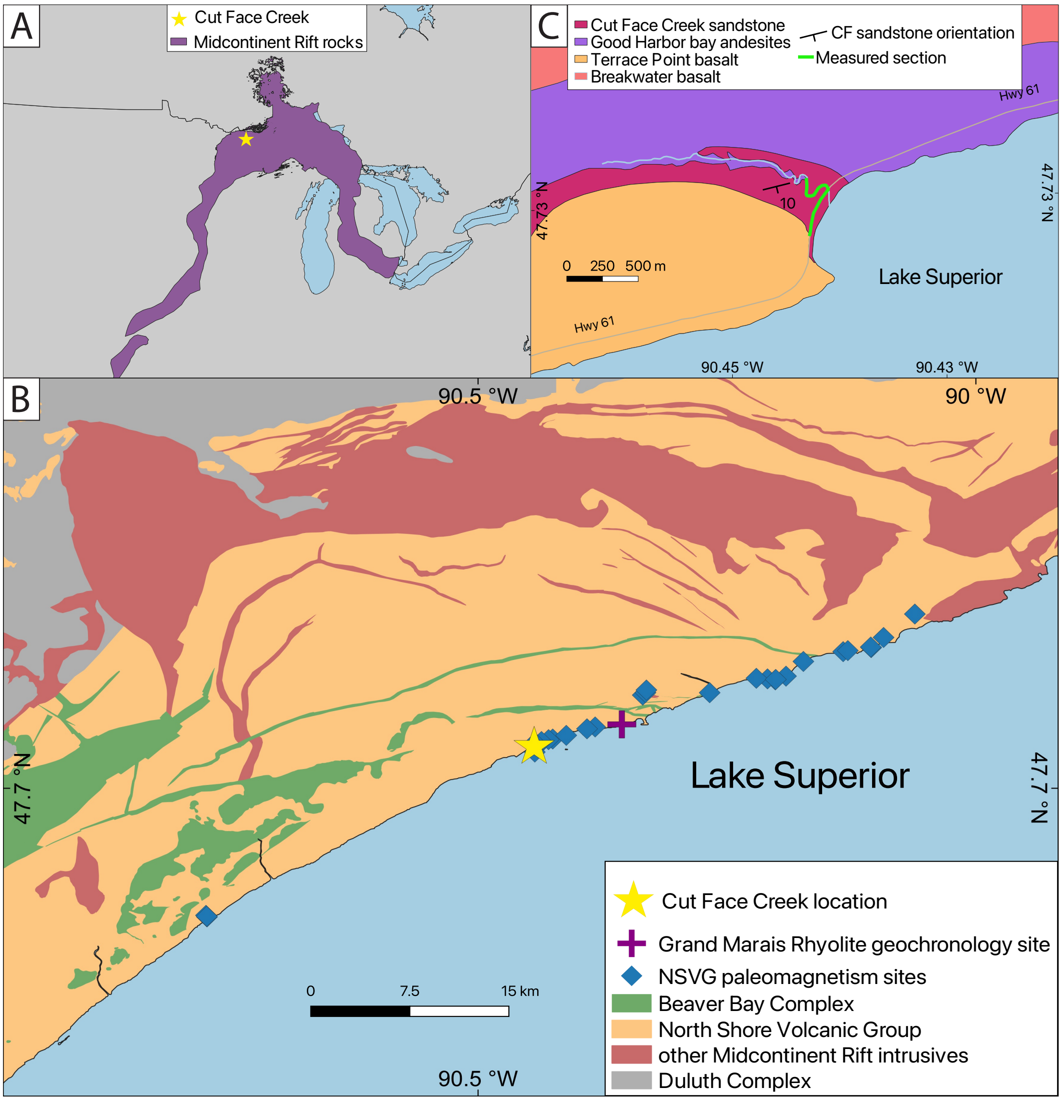

Figure 2: A) Overview map showing the location of the Cut Face Creek Sandstone (yellow star; 47.7280°N, 90.4428°W) within the extent of the Midcontinent Rift. B) Geologic map along the North Shore of Lake Superior showing the location of the Cut Face Creek Sandstone (yellow star) within the upper northeast sequence of the North Shore Volcanic Group (NSVG; geologic data from Miller et al. (2001)). CA-ID-TIMS ^{206}Pb/^{238}U dates constrain the Cut Face Creek Sandstone to be younger than the 1093.52 ± 0.43 Ma Grand Marais Rhyolite (purple cross; Swanson-Hysell et al. (2019)) and older than the 1091.7 Ma ± 0.2 Ma cross-cutting Beaver River diabase of the Beaver Bay Complex (green unit, Zhang et al. (2021)). C) The Cut Face Creek Sandstone overlies the Good Harbor Bay andesite (purple) while the Terrace Point basalt (tan orange) erupted atop the sandstone. The green line indicates the location of the measured stratigraphic section shown in Fig. 3.

overflows its channel leading to overbank deposition (e.g. van Toorenenburg et al., 2018). The next ∼11.8 m of strata continue to fine upwards and are dominated by very fine to fine-grained sandstone containing interbeds of cm-scale siltstone. This interval, which contains siltstone rip-up clasts and current ripples with variable flow directions (Fig. 3),

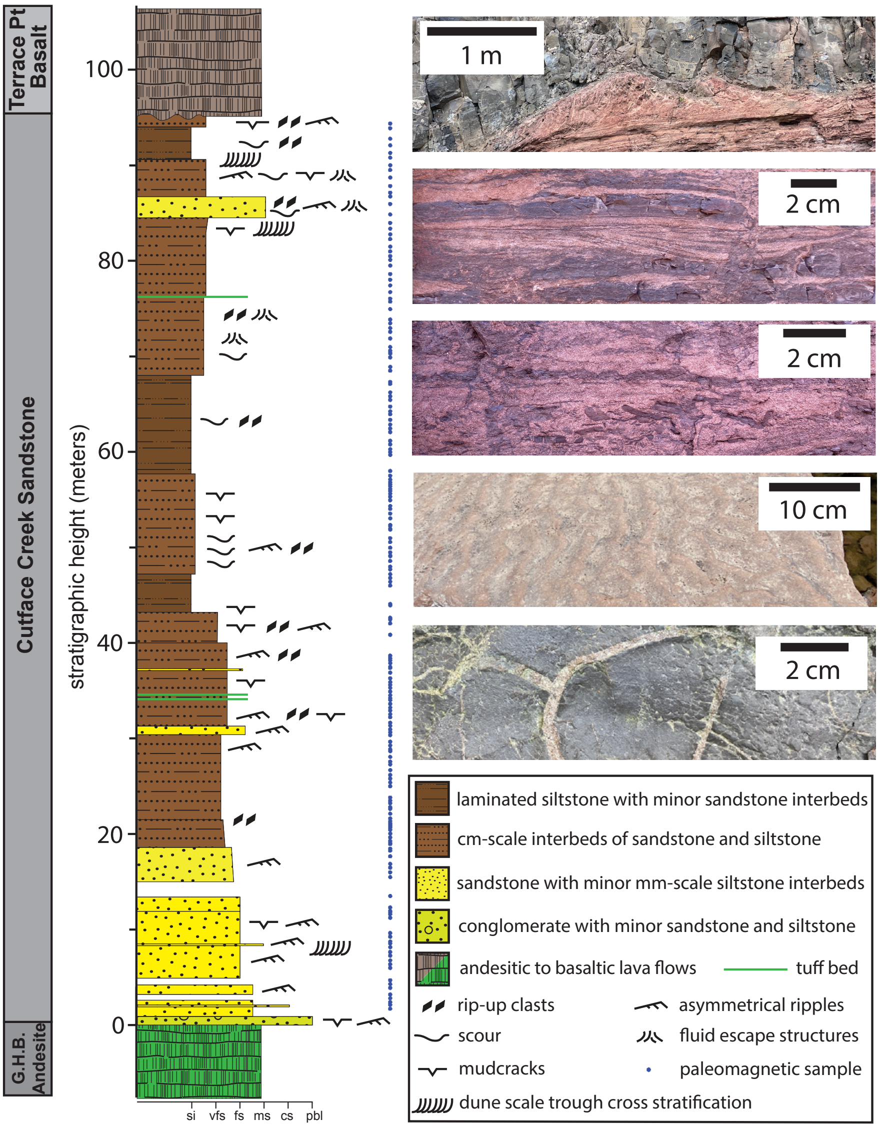

Figure 3: Stratigraphic column of the 95-meter-thick Cut Face Creek Sandstone as exposed along Cut Face Creek and Hwy 61 (Fig. 2). The Cut Face Creek Sandstone was deposited during a hiatus in eruption of the lavas North Shore Volcanic Group such that it is bracketed by the Good Harbor Bay andesites (G.H.B.; green) and the Terrace Creek Basalt (grey). Photos from bottom to top: top view of a mud-cracked siltstone layer within the basal conglomerate; oblique top view of current ripples in sandstone; side view of sandstone (light red) with tabular rip-up clasts of siltstone (dark red); side view of finely interbedded siltstone (dark red) and sandstone (light red) with asymmetric scour and ripple cross-stratification with fluid escape structures; upper contact with Terrace Point Basalt whose advance led to soft sediment deformation in the underlying Cut Face Creek Sandstone.

is characteristic of continued aggradation of crevasse splay deposits situated farther from the fluvial channel than the underlying interval. At 30.4 m, the stratigraphic trend is disrupted by a similar fining-upwards interval with a basal 1.1 m layer of medium-grained sandstone containing current ripples grading up into ~11.7 m of fine to very fine-grained sandstone with regular interbeds of cm-scale siltstone, which by the top of the interval are subequal in thickness. This interval contains cream-colored ash beds, mudcracks, current ripples, and siltstone rip-up clasts consistent with an increasingly distal overbank environment. The overlying ∼41.3 m of strata is dominated by laminated siltstone, and contains regular occurrences of mudcracks and siltstone rip-up clasts—consistent with floodplain sedimentation. Within this interval, fine-grained sandstone is deposited in cm-scale sheets characteristic of distal crevasse splay flooding events and in decimeter-scale asymmetric scours characteristic of meandering channels within a floodplain (Cant & Walker, 1976), with the latter occasionally infilled by dune-scale trough cross-bedding. The upper ∼15 m of the siltstone-dominated interval, coarsens upwards, and contains strata that can be disrupted by dewatering structures and infilled cracks that may be attributed to a combination of desiccation, shrinkage, and compaction (Fig. 3). The upper ∼10.6 m of the stratigraphic section coarsens upwards from ∼30% siltstone to well-lithified fine- to medium-grained sandstone, which was likely deposited in a crevasse splay environment in proximity to a fluvial channel. Flame structures associated with dewatering are common throughout the top part of the section (Fig. 3) with some ripple-scale cross-bedding. The uppermost 5 m include light tan colored horizons (Fig. 3) associated with fluid flow and reduction of the pigmentary hematite. The top 1.1 m beneath the Terrace Point basalt consists of baked siltstone with mudcracks and slaty cleavage. Eruption of the overlying lava flow of the Terrace Point basalt folded and deformed the uppermost sediment layers as it advanced and "bulldozed" the unconsolidated sediment (Fig 3).

Overall, these observations and interpretations are consistent with those of Jirsa (1984) and Mitchell and Sheldon (2009) who invoke a fluvial depositional environment dominated by overbank deposition. Flow in this fluvial system was dominantly to the SSW with the composition of sandstone consistent with a provenance largely derived from the local North Shore Volcanic Group (Jirsa, 1984).

3 Methods

Paleomagnetic cores from the Cut Face Creek Sandstone were sampled through the strata with an interval of ∼50 cm (Fig. 3). In order to maximize sampling of paleosecular variation, we optimized for vertical stratigraphic coverage and collected one sample at each horizon. As such, each sample constitutes a paleomagnetic site considering that a paleomagnetic site (which ideally captures a single snapshot of the local geomagnetic field) is a particular bed in a sedimentary sequence. Dark red fine-grained siltstone layers were preferentially sampled as they have lower permeability and are less susceptible to diagenetic alteration through fluid flow than coarser grained sandstone. Care was taken to avoid samples containing reoriented siltstone rip-up clasts from underlying strata. Paleomagnetic samples were oriented using a magnetic compass and a sun compass whenever possible. Sun compass data were preferentially used when available.

The specimens underwent step-wise thermal demagnetization in the UC Berkeley Paleomagnetism Lab using an ASC demagnetizer (residual fields <10 nT) with measurements of remanent magnetization made on a 2G DC-SQUID magnetometer. The demagnetization protocol had increasingly high-resolution steps (5 to 2°C) approaching the Néel temperature of hematite (up to ∼687°C). Implementing these high-resolution thermal demagnetization steps allowed us to isolate magnetic remanence components carried by coarser detrital hematite grains from finer pigmentary hematite grains (Fig. 4; Swanson-Hysell et al. (2019)). Least-squares fits were made to distinct components (Kirschvink, 1980) using PmagPy (Tauxe et al., 2016). All paleomagnetic data are available to the measurement level in the MagIC database (`https://earthref.org/MagIC/19603/789b4868-fb73-4315-af37-81f599cacc4a`; this link is for review purposes and will be updated when the manuscript is given a doi).

4 Results and Interpretation

4.1 Thermal demagnetization

High-resolution thermal demagnetization on the Cut Face Sandstone reveals three magnetization components: a low-temperature component that typically unblocks up to 200°C, a mid-temperature component that was typically removed up to 650°C, and a high-temperature component that was typically removed between 650°C and 687°C (Fig. 4). In the specimen demagnetization data, there is typically a shallowing of inclination from the mid-temperature component to the high-temperature component (Fig. 4). The high unblocking temperature range for the high temperature component is consistent with the interpretation that it is held by hematite grains that have sizes >400 nm and have unblocking temperatures close to the Néel temperature of hematite (Jiang et al., 2015; Swanson-Hysell et al., 2019). We interpret the high-temperature component to be a detrital remanent magnetization (DRM) acquired at the time of Cut Face Creek Sandstone deposition. In contrast, the relatively lower unblocking temperatures and generally steeper inclinations for the mid-temperature component is consistent with them being carried by pigmentary hematite grains of smaller sizes (<400 nm) that record a chemical remanent magnetization (CRM) during their growth within the sediment soon after deposition (Swanson-Hysell et al., 2019). Of the 179 samples analyzed from the Cut Face Creek Sandstone, a high-temperature component was resolved in 157 specimens, while a mid-temperature component was resolved in 167 specimens, and a low-temperature component in 109 specimens (Fig. 4).

Fisher statistics were calculated to obtain mean directions for each component. In geographic coordinates not corrected for bedding tilt, the mean low-temperature component has a declination of 359.3° and an inclination of 67.2° (α_{95}=2.0; k=46.0; n=109; Fig. 4). This direction is indistinguishable from the local expected dipole field (dec=000.0°, inc=65.6°) consistent with it being a recently acquired viscous remanent magnetization. The bedding tilt-corrected mid-temperature component has a mean declination of 286.5° and an inclination of 42.0° (α_{95}=1.6; k=48.2; n=167). This direction is indistinguishable from the mean direction of the lava flows of the upper northeast sequence of the North Shore Volcanic Group (dec=290.7°; inc=41.4° α_{95}=4.9°; n=28; Swanson-Hysell et al. (2019); Fig. 5) as they pass a statistical common mean test. This directional similarity is consistent with the interpretation that the pigmentary hematite grains within the Cut Face Creek Sandstone formed soon after deposition as a CRM and did not experience shallowing following formation. The tilt-corrected high-temperature component has a mean declination of 286.6° and an inclination of 29.4° (α_{95}:=1.9; k=35.8; n=157). The high-temperature component has a nearly identical mean declination with that of the mid-temperature component, but its mean inclination is shallower than that of the mid-temperature component and that of the lava flows (Fig. 5). In addition to a shallower mean inclination, the shape of the distribution is skewed such that directions are more elongate towards the horizontal plane consistent with sedimentary inclination flattening (Tauxe and Kent (2004); resulting in an elongation axis trending NE-SW for this data set; Fig. 4). This elongation contrasts with that of the mid-temperature component which is elongate in the vertical plane (an elongation axis trending NW-SE for this data set) as expected for an unflattened distribution of directions (Fig. 4). Taken together with the unblocking temperatures consistent with detrital hematite, the shallowed inclination and

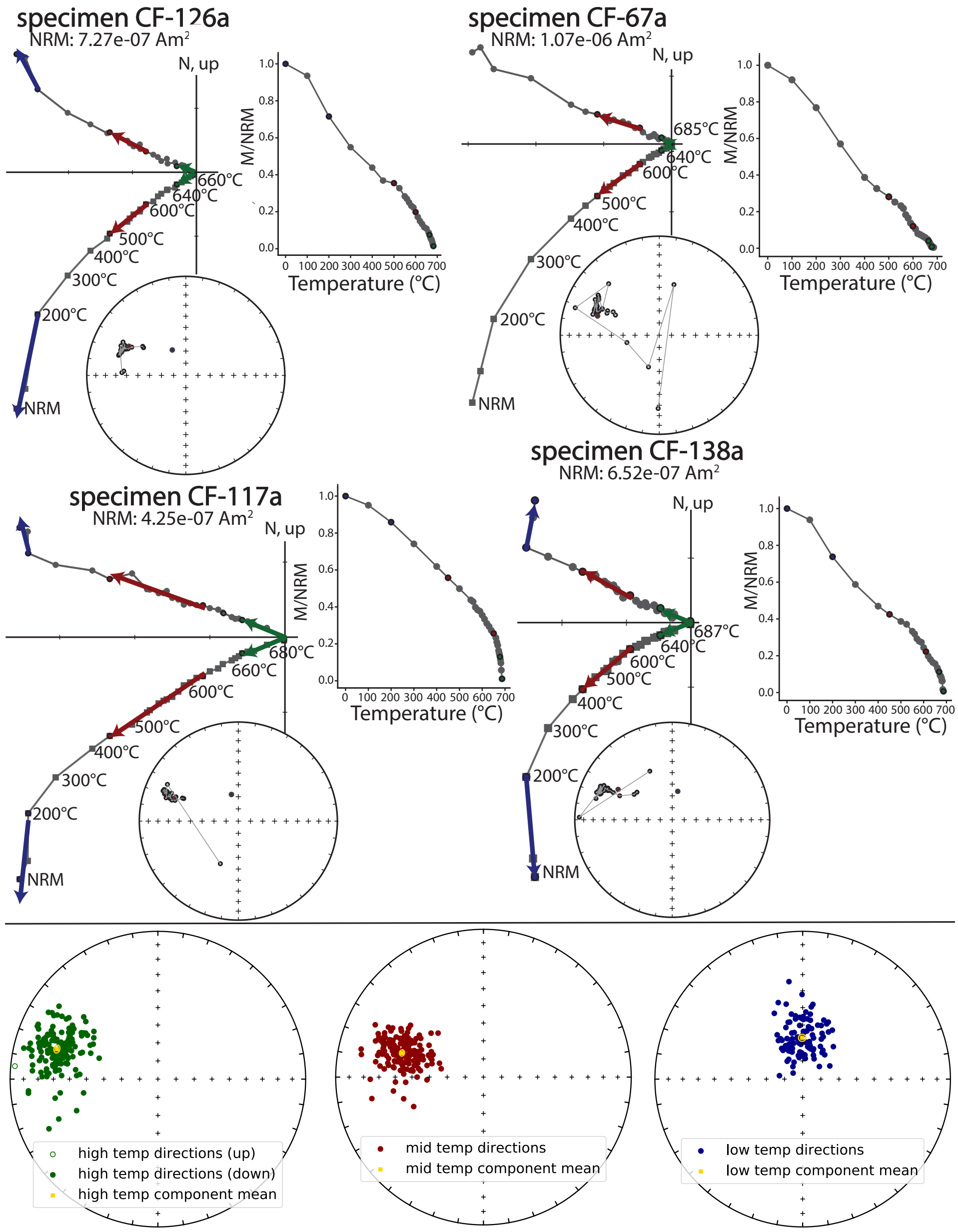

Figure 4: Example specimen thermal demagnetization results (top panel) and summary of all remanence components on equal area plots (bottom panel). The vector orthogonal plots show progressive magnetization direction changes through high-resolution demagnetization. The low-temperature component (blue) with a northerly declination and steep downward inclination is interpreted to have been acquired recently as its direction is indistinguishable from the present local axial dipole field. The mid-temperature component (red) is interpreted to be a chemical remanent magnetization (CRM) acquired soon after deposition of the Cut Face Creek Sandstone and was not flattened. The high temperature component (green) is interpreted as a detrital remanent magnetization (DRM) acquired through sediment deposition that was shallowed due to depositional and post-depositional processes.

the distribution shape indicate that the high-temperature magnetization is a detrital remanent magnetization.

4.2 Empirical inclination shallowing assessment

Given that the true paleomagnetic direction at the time of Cut Face Creek Sandstone deposition can be constrained by the records of the bracketing North Shore Volcanic Group and the sandstone's CRM directions which are not shallowed (i.e. they share a common mean with the volcanic directions; Fig. 5A), we can empirically determine the degree of inclination shallowing of the DRM and compare the results with that from the statistical E/I method (Tauxe & Kent, 2004).

Given that there are uncertainties associated with each mean direction, there will be a range of f factors that will steepen the DRM direction to share a common mean with the directions that are not shallowed. To determine this range, we incrementally corrected all specimen DRM directions by an f factor ranging from 1 to 0 with a step size of 0.001 (Fig. 5). As f decreases from 1 to 0 (i.e. the amount of unflattening increases), it is observed that the angles between the mean direction of the corrected DRM directions and those of both the CRM directions and the lava flow directions decrease toward a minimum when f is around 0.6, which is followed by an increase as the directions are steepened toward vertical (Fig. 5). In addition to calculating the angle between the mean of the corrected DRM directions and the means of the CRM and lava directions, we conducted common mean tests at each f factor (McFadden and McElhinny (1990); Fig. 5). In each iteration, the f factor is deemed plausible if the null hypothesis that the two populations share a common mean cannot be rejected. An f factor of 0.65 minimizes the angle between the DRM and the volcanic directions (3.6° angular difference) with the populations having statistically indistinguishable populations (i.e. passing a common mean test) between f factors of 0.75 and 0.56 (Fig. 5D). An f factor of 0.61 minimizes the angle between the DRM and CRM (0.01° angular difference) with statistically indistinguishable directions between 0.67 and 0.55 (Fig. 5C). These empirical f factors are similar (Fig. 5E) with the uncertainty of the f factor determined through the DRM to CRM comparison being smaller due to the higher number of vectors in the CRM population (n=167) than in the volcanics population (n=28).

As an additional analysis, we grouped the specimens by grain size and compared the specimen DRM directions to the volcanic directions. This analysis revealed claystone/siltstone to have been shallowed the most ($f = 0.56^{0.67}_{0.47}$), followed by the very fine-grained sand-

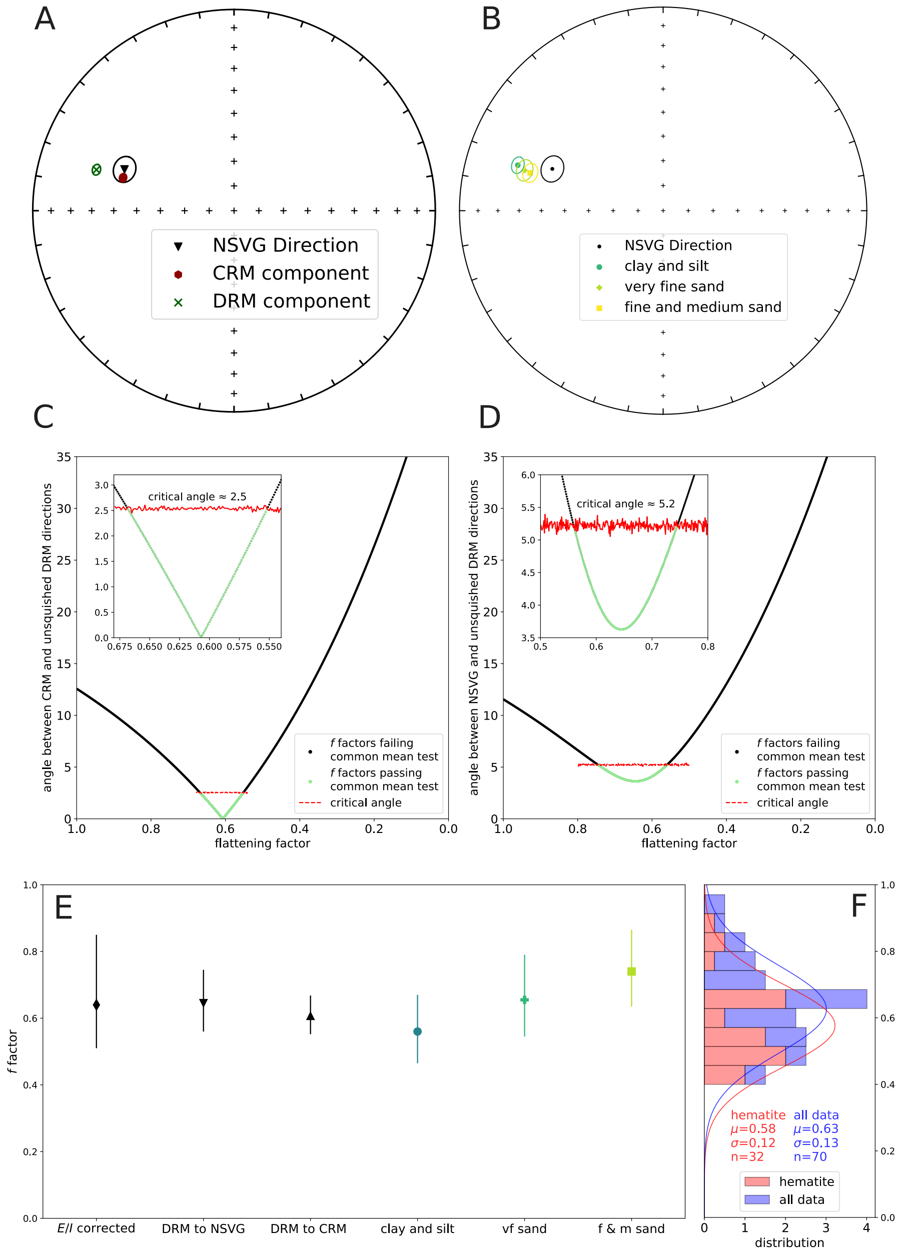

Figure 5: (A) Equal area plot comparing mean directions of Cut Face Creek Sandstone CRM and DRM magnetizations with that of the upper northeast sequence of the North Shore Volcanic Group (NSVG; Swanson-Hysell et al. (2019)). The mean CRM direction is indistinguishable from the volcanic direction while the DRM is shallowed relative to both. (B) Equal area plot comparing DRM directions of specimens grouped by grain size. Finer grain sizes have experienced more inclination shallowing. (C, D) Flattening factor estimates determined by progressively unflattening DRM directions and performing common mean tests between the DRM directions corrected by a given f factor and the CRM directions (in C) and the volcanics directions (in D). Green points are those that resulted in a statistically indistinguishable common mean (McFadden & McElhinny, 1990). The f factor resulting in the smallest angles and these common mean f factor test ranges for both DRM to NSVG volcanics and DRM to CRM are shown in (E) along with the f factor estimated using the E/I method and its associated 95% confidence bounds (Fig. 6). Also shown are the f factors and ranges for the DRM directions grouped by grain size compared to the NSVG directions. The stacked histogram in (F) summarizes compiled f factors for hematite-bearing sedimentary rocks as well as magnetite/mixed detrital magnetic mineralogy on the same axis as the estimates from this study in (E). A normal distribution fit to the f factors for hematite-bearing rocks has a mean of 0.58 with 1σ of 0.12. A normal distribution fit to magnetite and hematite data has a mean of 0.63 with 1σ of 0.13.

stones ($f = 0.66^{0.79}_{0.55}$), with the inclinations of specimens of medium- to fine-grained sandstone being the least shallowed ($f = 0.74^{0.87}_{0.64}$) (Fig. 5B,E).

4.3 Elongation/inclination flattening assessment

Applying the statistical E/I method to estimate the extent of inclination shallowing yielded an f factor of 0.64 with a 95% confidence range of 0.85 to 0.51 (Fig. 6). This uncertainty range is determined through 5,000 bootstrap resamples. The f factor estimate of $0.64^{0.85}_{0.51}$ obtained using the E/I method is very similar to that obtained empirically through the comparison of the DRM to the volcanics ($f = 0.65^{0.75}_{0.56}$) and the DRM to the CRM ($f = 0.61^{0.67}_{0.55}$) albeit with large associated uncertainty.

5 Discussion

5.1 Inclination shallowing in hematite-bearing sedimentary rocks

As has been long demonstrated in experimental and field studies (e.g. Tauxe & Kent, 1984; Lovlie & Torsvik, 1984), our study found that the remanence held by detrital hematite was shallowed with respect to the field in which it was acquired. In contrast, the remanence held by pigmentary hematite recovered the expected direction. The rapid accumulation of subsequent lava flows within the North Shore Volcanic Group may have accelerated the chemical transformation to pigmentary hematite of precursor iron oxide phases such as ferrihydrite such that it occurred soon (<1 Myr) after deposition. In this case, it is both interesting and useful that the CRM held by the pigmentary hematite returns the expected direction. However, since it is inherently a secondary phase that could be acquired on varied timescales, we caution against this result being broadly extrapolated to other formations. As was found in the study of siltstone intraclasts by Swanson-Hysell et al. (2019), high-resolution thermal demagnetization steps are necessary to isolate the DRM from the CRM. Isolating DRM held by detrital hematite is quite important if one is then applying an inclination flattening correction given that the CRM of pigmentary hematite is not expected to be flattened as shown in this study.

The f factors determined in this study of $f = 0.65^{0.75}_{0.56}$ for the comparison of the DRM to the volcanics, $f = 0.61^{0.67}_{0.55}$ for the comparison of the DRM to the CRM, and $0.64^{0.85}_{0.51}$ through the E/I method are all similar to one another (Fig. 5E). In addition, they overlap with compiled f factors in the literature for hematite-bearing sedimentary

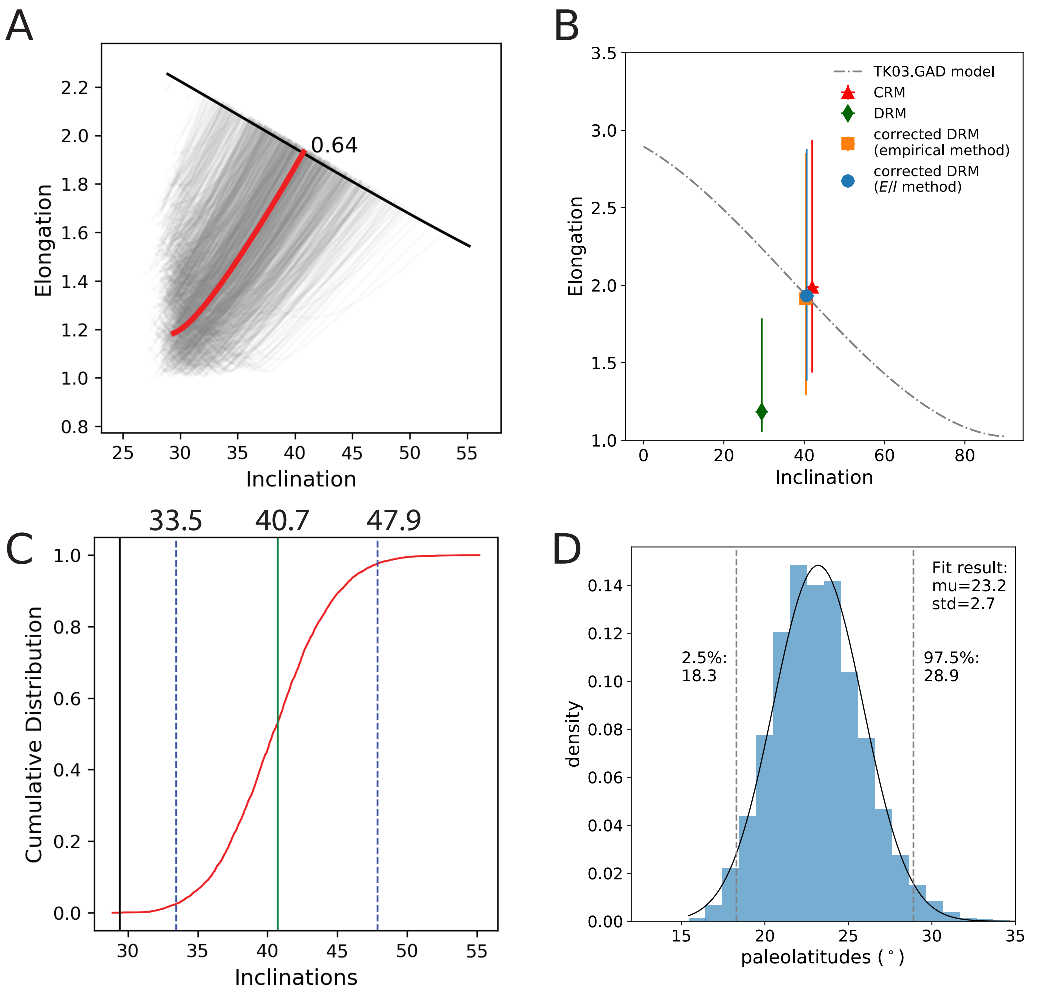

Figure 6: Results of the estimated amount of inclination shallowing of the detrital remanent magnetization of the Cut Face Creek sandstone using the elongation/inclination method (Tauxe & Kent, 2004). (A) The E/I method results in an estimated flattening factor of f=0.64 (red curve) based on where elongation/inclination intersects that predicted by the TK03 paleosecular variation model (black curve). The grey lines show the analysis applied to 5,000 bootstrap resamples of the DRM directions of the Cut Face Creek Sandstone which provide an estimate of the uncertainty associated with the f factor estimate. B) The distribution of the CRM vectors (red triangle) as well as those for the DRM corrected with f=0.65 (value that minimize the angle between the mean of the corrected DRM and the mean pole of the NSVG lava flows; orange square) have E/I values that are very close to that predicted by TK03.GAD. The DRM vectors corrected by the E/I method (blue circle) are directly on the TK03.GAD curve by definition of the method. C) The cumulative distribution of all plausible inclinations based on the E/I bootstrap results. D) The distribution of the paleolatitudes implied from the inclinations that result from the E/I method bootstrap resamples. The 95% confidence range spans a range of paleolatitudes that needs to be incorporated into the uncertainty on the resulting paleomagnetic pole.

rocks (Fig. 5F). One approach that has been taken in the literature is to assume an f factor of 0.6 and apply that to sedimentary poles for which no study specific factor was determined (Domeier et al., 2012; Torsvik et al., 2012). This assumed value was informed through a compilation of f factors developed using anisotropy approaches and the E/I method that was presented in Bilardello and Kodama (2010c). The f factor determined empirically for the Cut Face Creek Sandstone in this study is quite close to the assumed value of 0.6 applied to sedimentary paleomagnetic data by (Torsvik et al., 2012). However, numerous studies (e.g. Bilardello and Kodama (2010c) and Ding et al. (2015)) have cautioned against applying an assumed f factor and the variability in f factors between formations and within individual formations continues to be highlighted as inconsistent with a single value (e.g. Vaes et al., 2021). Our data corroborate this perspective as they reveal a relationship where the finer grained clay and siltstone lithologies are more flattened than the sandstone lithologies highlighting the variability of flattening in clastic sedimentary rocks as discussed in more detail below (Fig. 5).

5.2 Implications for applying the TK03 model and the E/I method in deep time

The TK03 model for paleosecular variation, and therefore the target inclination-elongation curve that is used in the E/I method, was developed to match the variation of scatter within a compilation of lava flows for the past 5 Myr (McElhinny & McFadden, 1997; Tauxe & Kent, 2004). It remains an open question whether this model is representative of the field at times further back in Earth history. There is support that comes from compilations of data from large igneous provinces over the Phanerozoic Era, and back to the 1.1 Ga Midcontinent Rift, that yield inclination-elongation relationships consistent with that predicted by the model (Tauxe et al., 2008; Tauxe & Kodama, 2009). Additionally, comparisons between sedimentary inclinations corrected through the E/I method and coeval volcanics have been shown to yield consistent results in multiple studies including ca. 200 Ma (Kent & Olsen, 2008) and ca. 50 Ma (Vaes et al., 2021).

In our study, the close correspondence of the f factor determined through the E/I method and the empirical approach (Fig. 5E) supports the application of E/I at this time in the late Mesoproterozoic Era (the Stenian Period). A caveat to this conclusion is that there is large uncertainty on the f factor coming out of the bootstrap analysis as is typical when applying the E/I method to paleomagnetic data sets which limits the precision of the comparison. These uncertainties arise from the the reality that the shape of a distribution is more uncertain and prone to variability through bootstrap resampling than the mean of a distribution.

Another way to evaluate the applicability of the TK03 model in the late Mesoproterozoic is to consider the shape of the distribution of CRM directions (Fig. 6). These directions represent unflattened magnetization acquired as pigmentary hematite was growing within the sediment following deposition (likely from precursor ferric oxide phases). The relationship of the elongation and the unflattened inclination recorded by the pigmentary hematite corresponds closely with that of the TK03.GAD model (Fig. 6B). While there is appreciable uncertainty on the elongation estimate through this analysis (as represented in the bootstrap determined confidence bounds in Fig. 6B), it provides additional support for applying the TK03.GAD model in deep time.

5.3 Uncertainty in flattening factor estimates

Uncertainty is inherent to any method of estimating a flattening factor. Even in the case of an empirical flattening analysis with comparison to well-constrained unflattened time-equivalent directions as in this study, the uncertainty on mean directions leads to a range of plausible f factors (as determined through the common mean tests shown in Fig. 5). This range is more dramatic when the E/I method is applied given the limitations in tightly constraining the shape of a distribution from a population of vectors at a number that is feasible to obtain through paleomagnetic study. Correcting the DRM directions by the f values of 0.85 and 0.51 at the bounds of the 95% confidence interval found through E/I analysis (Fig. 6) will result in two distinct direction distributions (i.e. they fail a common mean test) whose mean directions are 13.3° apart. Such an angular difference in directional space translates into a 9.7° difference in calculated pole positions for the Cut Face Creek Sandstone. This difference highlights that such uncertainty on inclination needs to be incorporated into mean paleomagnetic poles developed from sedimentary rocks.

In addition to data analysis challenges which lead to inescapable uncertainty, there is also the reality that a sedimentary unit will have varying flattening factors in different horizons. Variability in ferromagnetic mineral assemblages, sedimentary grain size, and depositional processes —all of which are expected within a sedimentary formation— will impact flattening. The variability in inclination shallowing as a function of grain size has been shown in redeposition experiments such as those conducted by Tan et al. (2002) on disaggregated red beds. Their finding that deposits of finer grain size are more prone to inclination shallowing is consistent with our finding of shallower inclination in siltstone than very fine sandstone which in turn is more shallowed than fine to medium sandstone (Fig. 5B).

Despite expected variability in flattening factors within a single sedimentary rock unit and inherent uncertainty in methods of determining f factors, studies typically use a single f factor to correct for inclination shallowing. This approach holds true both in studies that assume a single f factor (e.g. 0.6 applied to all sedimentary poles; Torsvik et al. (2012)) as well as in studies that develop estimates through anisotropy approaches or the E/I method both of which have associated uncertainty. In the case of the E/I method, researchers often consider the resulting f factor but do not incorporate the associated bootstrap uncertainty bounds when interpreting the data and developing associated paleomagnetic poles.

5.4 Better representing inclination shallowing uncertainties in sedimentary paleomagnetic poles

Given that there is uncertainty in f factor regardless of method, this uncertainty needs to be incorporated into the uncertainty on the mean pole position developed from detrital remanent magnetization in sedimentary rocks. While paleomagnetic poles are typically represented by circularly symmetric Fisher distributions, uncertainty in f factor will increase uncertainty in the direction between an unflattened paleomagnetic pole and the study site such that the spherical uncertainty region is elliptical.

A strength of the E/I method is that the bootstrap approach to determine uncertainty returns an ensemble of f factors that represents the uncertainty on the inclination correction. In Figure 6D, we show the distribution of paleolatitudes that results from applying these f factors to variably correct the shallowed Cut Face Creek Sandstone DRM. The resulting paleolatitude distribution can be approximated by a normal distribution (mean=23.2°N; one standard deviation=2.7°; Fig. 6D). A Kent distribution implements a bivariate normal distribution on a sphere which can therefore represent increased uncertainty in the colatitude direction (the conjugate of paleolatitude) between the study site and the paleomagnetic pole. The distribution shown in Fig. 6D has a heavy tail given the transformation of directions to pole space such that representation with a normal distribution is an approximation. However this is a useful approximation, as the Kent

475 distribution provides a succinct way to summarize the uncertainties associated with sed-
476 imentary paleomagnetic poles that include f factor uncertainty.

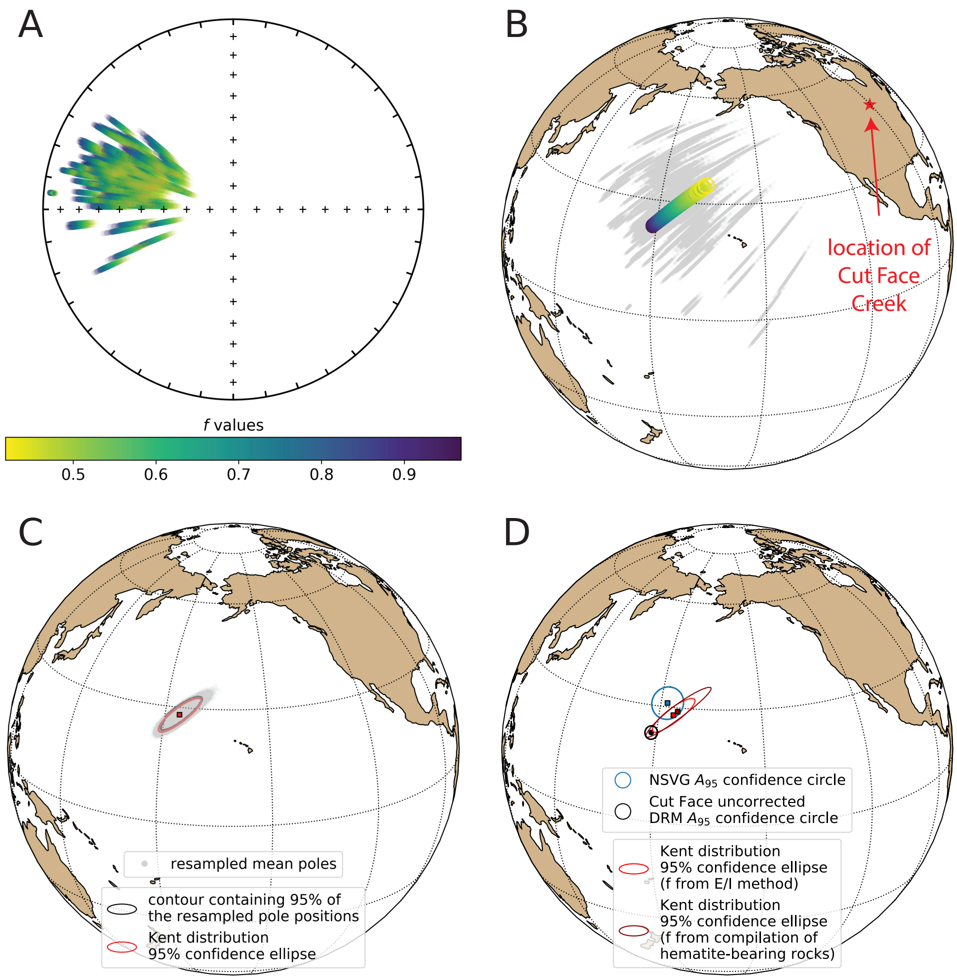

Figure 7: A new method for incorporating inclination shallowing uncertainty into sedimentary paleomagnetic poles. With each of the 5,000 f values determined from the E/I method bootstrap resampling routine (Tauxe & Kent, 2004), we corrected all Cut Face Creek Sandstone DRM directions (shown colored by f factor in (A) and calculated their associated virtual geomagnetic pole positions (grey points in B). Mean pole positions with associated A_{95} calculated with Fisher statistics are shown in (B) also color-coded by the f factor that leads to that pole. To characterize the distribution shape, we Monte-Carlo resampled 100 random inclination-corrected mean pole positions from the angular standard deviation (θ_{95}) of the Fisher mean pole associated with each f value. The total 500,000 Monte-Carlo resampled results on the mean pole positions are shown as grey points in (C) along with the contour that encapsulates 95% of the resampled mean poles (in black). Also shown is the 95% confidence ellipse of the Kent distribution (red ellipse) which closely matches the 95% contour indicating that it is an effective summary of the distribution. The Kent distribution confidence ellipse for the Cut Face Creek pole that includes the f factor uncertainty resulting from the E/I method is shown in comparison with the North Shore Volcanic Group (NSVG) Fisher mean pole position in (D). Also, shown is the Kent distribution that results from applying the same approach with bootstrap resampled f factors taken from the compilation of published values. This approach could be applied to estimate the uncertainty of published sedimentary poles where E/I analysis is not possible.

To determine this uncertainty, we took all of the f factors from the E/I analysis (with 5,000 bootstrap resamples) and applied them to the DRM directions (Fig. 7A). Note that this can alternatively be done with a distribution of f factors associated with anisotropy uncertainty or from a compilation as discussed further below. For each f factor, we converted the directions to virtual geomagnetic poles (VGPs; grey in Fig. 7B) and calculated the mean paleomagnetic pole at each f factor as a Fisher mean (colored by f factor in Fig. 7B). What would typically be done with a single f factor (either calculated or assumed) is to take a single one of these poles as the resulting pole and report its Fisher mean which would underestimate uncertainty along the great circle between the pole and the study locality. Instead, we have an ensemble of possible poles associated with the ensemble of f factors. From these poles, we drew 100 random pole mean positions from each of the Fisher-distributed mean poles (grey poles in Fig. 7C). These resampled poles represent 500,000 possible mean pole positions and their elliptical distribution can be seen with the contour that contains 95% of the resampled mean pole positions (black curve in Fig. 7C). A Kent distribution calculated from these resampled mean poles that incorporates the flattening uncertainty is shown in red in Figure 7C and is very similar to the 95% contour. Kent distributions can be reported as the mean direction (γ_1), the major axis (γ_2) with a 95% semi-angle (ζ_{95}), and the minor axis (γ_3) with a 95% semi-angle confidence angle (η_{95}). The ellipse has its major axis along the great circle between γ_1 and γ_2 with its minor axis along the great circle between γ_1 and γ_3. The Kent mean ellipse for the Cut Face Creek Sandstone incorporating flattening uncertainty from the E/I method has a mean of Plon=184.4°E, Plat = 28.1°N, a major axis of γ_2=[297.9°E, 36.7°N] with a semi-angle of ζ_{95}=6.7° and a minor axis of γ_3=[67.3°E, 40.4°N] with a semi-angle of η_{95}=1.8°. The inclination corrected DRM Kent mean pole overlaps with the Fisher mean pole for the volcanics (Fig. 7).

For published datasets without estimates of inclination shallowing, one approach to incorporate the uncertainty associated with inclination shallowing is to use f factors from a compilation in contrast to assuming a single value (Bilardello & Kodama, 2008, 2009). Building on the compilations of Bilardello (2016) and Vaes et al. (2021), we compiled f factors from both anisotropy and E/I methods from clastic sedimentary rocks (Table S1). This compilation is summarized in the histogram in Figure 5F and Figure S1. The compilation reveals similar means and distributions between detrital magnetic mineralogies with slightly lower f values for hematite (Fig. 5F and Fig. S1). If an en-

Table 1: Kent mean paleomagnetic poles for the Cut Face Creek Sandstone

pole	mean pole position (Plon/Plat) γ_1	major axis γ_2	major axis 95% confidence angle ζ_{95}	minor axis γ_2	minor axis 95% confidence angle η_{95}
Cut Face E/I corrected	184.4°E / 28.1°N	297.9°E / 36.7°N	6.7°	67.3°E / 40.4°N	1.8°
Cut Face compilation corrected	185.7°E / 29.3°N	299.8°E / 36.0°N	10.8°	67.6°E / 40.1°N	1.7°

Notes: The Fisher mean of the Cutface Creek paleomagnetic pole without an inclination shallowing correction is Plon=178.5, Plat=23.0, A_{95}=1.7; the values associated with the compilation correction can slightly change with different bootstrap resampling runs given the relatively low number of f factors in the compilation.

semble of f factors resulting from the EI method is not available for a sedimentary paleomagnetic pole, these compiled f factors could be used to estimate the uncertainty associated with inclination shallowing and develop a Kent distribution pole. To do so, we follow the same approach described above with the modification of using f factors that are drawn from bootstrap resampling from the compilation. As is visualized in Figure 7D, the resulting uncertainty ellipse is larger than that when f factors come from the E/I analysis given that our knowledge of the inclination shallowing is less informed and taken from all estimated f factors. The Kent means and associated statistics resulting from applying the E/I correction and the compilation-based correction to the Cut Face Creek Sandstone are summarized in Table 1. Applying this method to synthetic and other sedimentary datasets yields similarly reasonable results as shown in the archived Jupyter notebooks accompanying this work.

Incorporating inclination shallowing uncertainty into the presentation of mean paleomagnetic poles has several advantages. It more completely communicates the uncertainty associated with paleomagnetic poles developed from detrital remanent magnetization. Fisher mean paleomagnetic poles developed from sedimentary data often have small circular A_{95} confidence ellipses due to large numbers of samples in the mean. However, these small A_{95} uncertainty angles overestimate the confidence on the known position—particularly the co-latitude. Representing the uncertainty has the potential to reconcile disparate poles and address paleogeographic puzzles. Being able to approximate the mean pole position as a Kent distribution enables the mean pole and the uncertainty to be succinctly communicated. Additionally, the Kent distribution can be incorporated into frameworks such that probabilistic inversion or parametric Monte Carlo resampling can enable development of future apparent polar wander paths that incorporate uncertainty.

6 Conclusion

The Cut Face Creek Sandstone provides a 1.1-billion-year-old natural laboratory where the paleomagnetic pole position expected to have been recorded by the red beds can be tightly constrained by the lava flows that bracket it such that the amount of inclination shallowing of the sediments can be empirically determined. The statistical E/I method (Tauxe & Kent, 2004) yields an estimated range of f values for the hematite detrital remanent magnetization that agree with those derived empirically, but with larger uncertainties. Given that all methods have non-negligible uncertainties associated with determining the flattening factor, they should be recognized and incorporated into paleomagnetic syntheses. Incorporating uncertainty associated with inclination flattening leads to increased uncertainty in pole position between the unflattened pole position and the study site. We present a method that takes a range of unflattening factors and uses it to develop a mean pole and uncertainty ellipse that can be approximated as a Kent distribution. This method can be applied to datasets where f factors have been determined through E/I analysis as well as to datasets without such determination in which case the range of f factors can be taken from a literature compilation. Incorporating inclination shallowing uncertainty better represents our knowledge of ancient paleomagnetic pole positions thereby advancing paleogeographic reconstructions.

Acknowledgments

Support for this research came from NSF grant EAR-1847277 to Nicholas Swanson-Hysell and an UC Berkeley Summer Undergraduate Research Fellowship awarded to James Pierce.

Lisa Tauxe provided inspiration and feedback on the approach taken in this study. Margaret Avery provided feedback on an earlier draft of the manuscript. Sarah Swanson-Hysell and Madeline Swanson-Hysell assisted with fieldwork. Dario Bilardello provided a compilation of f factors associated with Bilardello (2016) that he updated to include more recent data for the talk "The Anisotropy Correction for Inclination Shallowing" presented at the 2021 Institute for Rock Magnetism Conference. Paleomagnetic data associated with this study are available within the MagIC database (https://earthref.org/MagIC/19603/789b4868-fb73-4315-af37-81f599cacc4a; UPDATE WHEN DOI IS GENERATED) and all data are within a Github repository associated with this work (https://github.com/Swanson-Hysell-Group/Inclination_Shallowing) that is also archived on Zenodo (https://doi.org/XXX; ZENODO RELEASE WILL BE MADE FROM GITHUB REPOSITORY UPON ACCEPTANCE). This repository also contains Python code that implements all of the calculations, visualizations and statistical tests discussed herein. We added to the Pmagpy Python package (Tauxe et al., 2016) a new function named *find_ei_kent* that finds the estimated range of plausible inclination shallowing factors for a set of sedimentary paleomagnetic directions using the E/I method and returns the associated Kent distribution that includes the uncertainty estimates from the E/I method to estimate the 95% confidence ellipse for a sedimentary paleomagnetic pole.

References

Anson, G. L., & Kodama, K. P. (1987). Compaction-induced inclination shallowing of the post-depositional remanent magnetization in a synthetic sediment. *Geophysical Journal International*, *88*(3), 673–692.

Bilardello, D. (2015). Isolating the anisotropy of the characteristic remanence-carrying hematite grains: a first multispecimen approach. *Geophysical Journal International*, *202*(2), 695–712. doi: 10.1093/gji/ggv171

Bilardello, D. (2016). The do's and don'ts of inclination shallowing corrections. *The IRM Quarterly*, *26*(3), 12.

Bilardello, D., Callebert, W. C., & Davis, J. R. (2018). Evidence for widespread remagnetizations in South America, case study of the Itararé Group rocks from the state of São Paulo, Brazil. *Frontiers in Earth Science*, *6*. doi: 10.3389/feart.2018.00182

Bilardello, D., & Kodama, K. (2008). Poster: A simplified red bed inclination correction: A case study from the permian esterel rocks of france. In *American Geophysical Union* (Vol. San Francisco, p. abstract id. GP51A-0733).

Bilardello, D., & Kodama, K. (2009). Poster: Magnetic fabric and inclination shallowing studies: depositional and post-depostitional processes in hematite- and magnetite-bearing rocks. In *American Geophysical Union* (Vol. San Francisco, p. abstract id. GP43A-0841).

Bilardello, D., & Kodama, K. P. (2010a). A new inclination shallowing correction of the Mauch Chunk Formation of Pennsylvania, based on high-field AIR results: Implications for the Carboniferous North American APW path and Pangea reconstructions. *Earth and Planetary Science Letters*, *299*(1-2), 218–227. doi: 10.1016/j.epsl.2010.09.002

Bilardello, D., & Kodama, K. P. (2010b). Palaeomagnetism and magnetic anisotropy of Carboniferous red beds from the Maritime Provinces of Canada: evidence for shallow palaeomagnetic inclinations and implications for North American apparent polar wander. *Geophysical Journal International*, *180*(3), 1013–1029. doi: 10.1111/j.1365-246X.2009.04457.x

Bilardello, D., & Kodama, K. P. (2010c). Rock magnetic evidence for inclination shallowing in the early Carboniferous Deer Lake Group red beds of western Newfoundland. *Geophysical Journal International*, *181*(1), 275–289. doi:

10.1111/j.1365-246X.2010.04537.x

Books, K. (1972). *Paleomagnetism of Some Lake Superior Keweenawan Rocks.* Geological Survey Professional Paper 760.

Butler, R. F. (1992). *Magnetic Domains to Geologic Terranes.* Blackwell Scientific Publications.

Cant, D. J., & Walker, R. G. (1976). Development of a braided-fluvial facies model for the Devonian Battery Point Sandstone, Québec. *Canadian Journal of Earth Sciences*, *13*(1), 102–119. doi: 10.1139/e76-010

Chen, W., Zhang, S., Ding, J., Zhang, J., Zhao, X., Zhu, L., ... Wu, H. (2017). Combined paleomagnetic and geochronological study on Cretaceous strata of the Qiangtang terrane, central Tibet. *Gondwana Research*, *41*, 373–389. doi: 10.1016/j.gr.2015.07.004

Costa, E., Garces, M., López-Blanco, M., Beamud, E., Gómez-Paccard, M., & Larrasoaña, J. C. (2009). Closing and continentalization of the South Pyrenean foreland basin (NE Spain): magnetochronological constraints. *Basin Research*. doi: 10.1111/j.1365-2117.2009.00452.x

Dallanave, E., Kirscher, U., Hauck, J., Hesse, R., Bachtadse, V., & Wortmann, U. G. (2018). Palaeomagnetic time and space constraints of the Early Cretaceous Rhenodanubian Flysch zone (Eastern Alps). *Geophysical Journal International*, *213*(3), 1804–1817. doi: 10.1093/gji/ggy077

Deenen, M. H. L., Langereis, C. G., van Hinsbergen, D. J. J., & Biggin, A. J. (2011). Geomagnetic secular variation and the statistics of palaeomagnetic directions. *Geophysical Journal International*. doi: 10.1111/j.1365-246X.2011.05050.x

Ding, J., Zhang, S., Chen, W., Zhang, J., Yang, T., Jiang, G., ... Wu, H. (2015). Paleomagnetism of the Oligocene Kangtuo Formation red beds (Central Tibet): Inclination shallowing and tectonic implications. *Journal of Asian Earth Sciences*, *104*, 55–68. doi: 10.1016/j.jseaes.2014.10.006

Domeier, M., Van der Voo, R., & Torsvik, T. H. (2012). Paleomagnetism and Pangea: The road to reconciliation. *Tectonophysics*, *514-517*, 14–43. doi: 10.1016/j.tecto.2011.10.021

Dupont-Nivet, G., Lippert, P. C., Hinsbergen, D. J. V., Meijers, M. J., & Kapp, P. (2010). Palaeolatitude and age of the Indo-Asia collision: palaeomagnetic constraints. *Geophysical Journal International*, *182*(3), 1189–1198. doi: 10.1111/j.1365-246x.2010.04697.x

Gallo, L. C., Tomezzoli, R. N., & Cristallini, E. O. (2017). A pure dipole analysis of the Gondwana apparent polar wander path: Paleogeographic implications in the evolution of Pangea. *Geochemistry, Geophysics, Geosystems*, *18*(4), 1499–1519. doi: 10.1002/2016gc006692

Green, J. C. (1983). Geologic and geochemical evidence for the nature and development of the middle Proterozoic (Keweenawan) Midcontinent Rift of North America. *Tectonophysics*, *94*(1), 413–437. doi: 10.1016/0040-1951(83)90027-6

Green, J. C., Boerboom, T. J., Schmidt, S. T., & Fitz, T. J. (2011). The North Shore Volcanic Group: Mesoproterozoic plateau volcanic rocks of the Midcontinent Rift system in northeastern Minnesota. *Archean to Anthropocene: Field Guides to the Geology of the Mid-Continent of North America: Geological Society of America Field Guide*, *24*, 121–146.

Gutiérrez, L., Barrón, V., Andrés-Vergés, M., Serna, C. J., Veintemillas-Verdaguer, S., Morales, M. P., & Lázaro, F. J. (2016). Detailed magnetic monitoring of the enhanced magnetism of ferrihydrite along its progressive transformation into hematite. *Journal of Geophysical Research: Solid Earth*, *121*(6), 4118–4129. doi: 10.1002/2016JB013016

Haldan, M. M., Langereis, C. G., Biggin, A. J., Dekkers, M. J., & Evans, M. E. (2009). A comparison of detailed equatorial red bed records of secular variation during the Permo-Carboniferous Reversed Superchron. *Geophysical Journal International*, *177*(3), 834–848. doi: 10.1111/j.1365-246x.2009.04124.x

Huang, W., Dupont-Nivet, G., Lippert, P. C., van Hinsbergen, D. J. J., & Hallot, E. (2013). Inclination shallowing in Eocene Linzizong sedimentary rocks from Southern Tibet: correction, possible causes and implications for reconstructing the India–Asia collision. *Geophysical Journal International*, *194*(3), 1390–1411. doi: 10.1093/gji/ggt188

Huang, W., van Hinsbergen, D. J., Maffione, M., Orme, D. A., Dupont-Nivet, G., Guilmette, C., . . . Kapp, P. (2015). Lower Cretaceous Xigaze ophiolites formed in the Gangdese forearc: Evidence from paleomagnetism, sediment provenance, and stratigraphy. *Earth and Planetary Science Letters*, *415*, 142–153. doi: 10.1016/j.epsl.2015.01.032

Jackson, M. J., Banerjee, S. K., Marvin, J. A., Lu, R., & Gruber, W. (1991). Detrital remanence, inclination Errors, and anhysteretic remanence anisotropy: Quantitative model and experimental results. *Geophysical Journal International*, *104*(1), 95–103. doi: 10.1111/j.1365-246X.1991.tb02496.x

Jiang, Z., Liu, Q., Dekkers, M. J., Tauxe, L., Qin, H., Barrón, V., & Torrent, J. (2015). Acquisition of chemical remanent magnetization during experimental ferrihydrite–hematite conversion in Earth-like magnetic field—implications for paleomagnetic studies of red beds. *Earth and Planetary Science Letters*, *428*, 1–10. doi: 10.1016/j.epsl.2015.07.024

Jiang, Z., Liu, Q., Roberts, A. P., Barrón, V., Torrent, J., & Zhang, Q. (2018). A new model for transformation of ferrihydrite to hematite in soils and sediments. *Geology*. doi: 10.1130/G45386.1

Jiang, Z., Liu, Q., Roberts, A. P., Dekkers, M. J., Barrón, V., Torrent, J., & Li, S. (2022). The magnetic and color reflectance properties of hematite: From Earth to Mars. *Reviews of Geophysics*, *60*(1). doi: 10.1029/2020rg000698

Jirsa, M. A. (1984). Interflow Sedimentary Rocks in the Keweenawan North Shore Volcanic Group, Northeastern Minnesota. *Minnesota Geological Survey*, 28.

Kent, D. V., & Olsen, P. E. (2008). Early Jurassic magnetostratigraphy and paleolatitudes from the Hartford continental rift basin (eastern North America): Testing for polarity bias and abrupt polar wander in association with the central Atlantic magmatic province. *Journal of Geophysical Research: Solid Earth*, *113*(B6). doi: doi.org/10.1029/2007JB005407

Kent, D. V., & Tauxe, L. (2005). Corrected late triassic latitudes for continents adjacent to the north atlantic. *Science*, *307*(5707), 240–244. doi: 10.1126/science.1105826

Kim, B., & Kodama, K. P. (2004). A compaction correction for the paleomagnetism of the Nanaimo Group sedimentary rocks: Implications for the Baja British Columbia hypothesis. *Journal of Geophysical Research: Solid Earth*, *109*(B2). doi: 10.1029/2003jb002696

King, R. F. (1955). The remanent magnetism of artificially deposited sediments. *Geophysical Supplements to the Monthly Notices of the Royal Astronomical Society*, *7*(3), 115–134. doi: 10.1111/j.1365-246X.1955.tb06558.x

Kirscher, U., Bilardello, D., Mikolaichuk, A., & Bachtadse, V. (2014). Correcting for inclination shallowing of early Carboniferous sedimentary rocks from Kyrgyzstan—indication of stable subtropical position of the North Tianshan Zone in the mid-late Palaeozoic. *Geophysical Journal International*, *198*(2), 1000–1015. doi: 10.1093/gji/ggu177

Kirschvink, J. L. (1980). The least-squares line and plane and the analysis of palaeomagnetic data. *Geophysical Journal International*, *62*(3), 699–718. doi: 10.1111/j.1365-246X.1980.tb02601.x

Kodama, K. P. (2009). Simplification of the anisotropy-based inclination correction technique for magnetite- and haematite-bearing rocks: a case study for the Carboniferous Glenshaw and Mauch Chunk Formations, North America. *Geophysical Journal International*, *176*(2), 467–477. doi: 10.1111/j.1365-246x.2008.04013.x

Kodama, K. P. (2012). *Paleomagnetism of sedimentary rocks: process and interpretation.* Chichester, West Sussex ; Hoboken, NJ: John Wiley & Sons.

Kodama, K. P., & Davi, J. M. (1995). A compaction correction for the paleomagnetism of the Cretaceous Pigeon Point Formation of California. *Tectonics*, *14*(5), 1153–1164. doi: 10.1029/95tc01648

Krijgsman, W., & Tauxe, L. (2004). Shallow bias in Mediterranean paleomagnetic directions caused by inclination error. *Earth and Planetary Science Letters*, *222*(2), 685–695. doi: 10.1016/j.epsl.2004.03.007

Krijgsman, W., & Tauxe, L. (2006). E/I corrected paleolatitudes for the sedimentary rocks of the Baja British Columbia hypothesis. *Earth and Planetary Science Letters*, *242*(1-2), 205–216. doi: 10.1016/j.epsl.2005.11.052

Lanci, L., Tohver, E., Wilson, A., & Flint, S. (2013). Upper Permian magnetic stratigraphy of the lower Beaufort Group, Karoo Basin. *Earth and Planetary Science Letters*, *375*, 123–134. doi: 10.1016/j.epsl.2013.05.017

Li, S., Li, Y., Tan, X., Wang, C., Han, Z., Xiao, S., … Zhang, J. (2022). New paleomagnetic results of the Upper Cretaceous to Lower Eocene sedimentary rocks from the Xigaze forearc basin and their tectonic implications. *Tectonophysics*, *837*, 229433. doi: 10.1016/j.tecto.2022.229433

Li, Y., Kodama, K., & Smith, D. (2001). A compaction-corrected inclination for the Middle Cretaceous Valle Group in Vizcaino Terrane, Baja California, Mexico: preliminary results. In *Agu fall meeting abstracts* (pp. GP41A–0256).

Lovlie, R., & Torsvik, T. (1984). Magnetic remanence and fabric properties of laboratory-deposited hematite-bearing red sandstone. *Geophys. Res. Lett.*, *11*(3), 221–224. doi: 10.1029/GL011i003p00221

Lu, H. M., & Meng, X. K. (2010). Morin temperature and Néel temperature of hematite nanocrystals. *The Journal of Physical Chemistry C*, *114*(49), 21291–21295. doi: 10.1021/jp108703b

McElhinny, M. W., & McFadden, P. L. (1997). Palaeosecular variation over the past 5 Myr based on a new generalized database. *Geophysical Journal International*, *131*(2), 240–252. doi: 10.1111/j.1365-246X.1997.tb01219.x

McFadden, P. L., & McElhinny, M. W. (1990). Classification of the reversal test in palaeomagnetism. *Geophysical Journal International*, *103*(3), 725–729. doi: 10.1111/j.1365-246X.1990.tb05683.x

Meijers, M. J. M., Kaymakci, N., van Hinsbergen, D. J. J., Langereis, C. G., Stephenson, R. A., & Hippolyte, J.-C. (2010). Late Cretaceous to Paleocene oroclinal bending in the central Pontides (Turkey). *Tectonics*, *29*(4). doi: 10.1029/2009tc002620

Meng, J., Coe, R. S., Wang, C., Gilder, S. A., Zhao, X., Liu, H., ... Li, S. (2017). Reduced convergence within the Tibetan Plateau by 26 Ma? *Geophysical Research Letters*, *44*(13), 6624–6632. doi: 10.1002/2017gl074219

Milanese, F., Rapalini, A., Slotznick, S. P., Tobin, T. S., Kirschvink, J., & Olivero, E. (2019). Late Cretaceous paleogeography of the Antarctic Peninsula: New paleomagnetic pole from the James Ross Basin. *Journal of South American Earth Sciences*, *91*, 131–143. doi: 10.1016/j.jsames.2019.01.012

Miller, J., James D., Green, J. C., Severson, M. J., Chandler, V. W., & Peterson, D. M. (2001). *M-119 Geologic map of the Duluth Complex and related rocks, northeastern Minnesota* (Tech. Rep.). Minnesota Geological Survey.

Mitchell, R., & Sheldon, N. (2009). Weathering and paleosol formation in the 1.1 Ga Keweenawan Rift. *Precambrian Research*, *168*(3-4), 271–283. doi: 10.1016/j.precamres.2008.09.013

Sun, W. W., & Kodama, K. P. (1992). Magnetic anisotropy, scanning electron microscopy, and X ray pole figure goniometry study of inclination shallowing in a compacting clay-rich sediment. *Journal of Geophysical Research: Solid Earth*, *97*(B13), 19599–19615. doi: 10.1029/92JB01589

Swanson-Hysell, N. L., Hoaglund, S. A., Crowley, J. L., Schmitz, M. D., Zhang, Y., & Miller, J. D. (2021). Rapid emplacement of massive Duluth Complex intrusions within the North American Midcontinent Rift. *Geology*. doi: 10.1130/G47873.1

Swanson-Hysell, N. L., Ramezani, J., Fairchild, L. M., & Rose, I. R. (2019). Failed rifting and fast drifting: Midcontinent Rift development, Laurentia's rapid motion and the driver of Grenvillian orogenesis. *GSA Bulletin*, *131*(5-6), 913–940. doi: 10.1130/B31944.1

Swanson-Hysell, N. L., Fairchild, L. M., & Slotznick, S. P. (2019). Primary and secondary red bed magnetization constrained by fluvial intraclasts. *Journal of Geophysical Research: Solid Earth*, *124*(5), 4276–4289. doi: 10.1029/2018JB017067

Tan, X., Gilder, S., Kodama, K. P., Jiang, W., Han, Y., Zhang, H., ... Zhou, D. (2010). New paleomagnetic results from the Lhasa block: Revised estimation of latitudinal shortening across Tibet and implications for dating the India–Asia collision. *Earth and Planetary Science Letters*, *293*(3-4), 396–404. doi: 10.1016/j.epsl.2010.03.013

Tan, X., & Kodama, K. P. (1998). Compaction-corrected inclinations from southern California Cretaceous marine sedimentary rocks indicate no paleolatitudinal offset for the Peninsular Ranges terrane. *Journal of Geophysical Research: Solid Earth*, *103*(B11), 27169–27192. doi: 10.1029/98jb02343

Tan, X., Kodama, K. P., Chen, H., Fang, D., Sun, D., & Li, Y. (2003). Paleomagnetism and magnetic anisotropy of Cretaceous red beds from the Tarim basin, northwest China: Evidence for a rock magnetic cause of anomalously shallow paleomagnetic inclinations from central Asia. *Journal of Geophysical Research: Solid Earth*, *108*(B2). doi: 10.1029/2001jb001608

Tan, X., Kodama, K. P., & Fang, D. (2002). Laboratory depositional and compaction-caused inclination errors carried by haematite and their implications in identifying inclination error of natural remanence in red beds. *Geophysical Journal International*, *151*(2), 475–486. doi: 10.1046/j.1365-246X.2002.01794.x

Tauxe, L. (2005). Inclination flattening and the geocentric axial dipole hypothesis. *Earth and Planetary Science Letters*, *233*(3-4), 247–261. doi: 10.1016/j

.epsl.2005.01.027

Tauxe, L., & Kent, D. V. (1984). Properties of a detrital remanence carried by haematite from study of modern river deposits and laboratory redeposition experiments. *Geophysical Journal International*, *76*(3), 543–561. doi: 10.1111/j.1365-246X.1984.tb01909.x

Tauxe, L., & Kent, D. V. (2004). A simplified statistical model for the geomagnetic field and the detection of shallow bias in paleomagnetic inclinations: was the ancient magnetic field dipolar? In *Geophysical Monograph Series* (pp. 101–115). American Geophysical Union. doi: 10.1029/145GM08

Tauxe, L., Kent, D. V., & Opdyke, N. D. (1980). Magnetic components contributing to the NRM of Middle Siwalik red beds. *Earth and Planetary Science Letters*, *47*(2), 279–284. doi: 10.1016/0012-821X(80)90044-8

Tauxe, L., & Kodama, K. P. (2009). Paleosecular variation models for ancient times: Clues from Keweenawan lava flows. *Physics of the Earth and Planetary Interiors*, *177*(1), 31–45. doi: 10.1016/j.pepi.2009.07.006

Tauxe, L., Kodama, K. P., & Kent, D. V. (2008). Testing corrections for paleomagnetic inclination error in sedimentary rocks: A comparative approach. *Physics of the Earth and Planetary Interiors*, *169*(1), 152–165. doi: 10.1016/j.pepi.2008.05.006

Tauxe, L., Shaar, R., Jonestrask, L., Swanson-Hysell, N. L., Minnett, R., Koppers, A. a. P., … Fairchild, L. (2016). PmagPy: Software package for paleomagnetic data analysis and a bridge to the Magnetics Information Consortium (MagIC) Database. *Geochemistry, Geophysics, Geosystems*, *17*(6), 2450–2463. doi: 10.1002/2016GC006307

Tong, Y., Yang, Z., Mao, C., Pei, J., Pu, Z., & Xu, Y. (2017). Paleomagnetism of Eocene red-beds in the eastern part of the Qiangtang Terrane and its implications for uplift and southward crustal extrusion in the southeastern edge of the Tibetan Plateau. *Earth and Planetary Science Letters*, *475*, 1–14. doi: 10.1016/j.epsl.2017.07.026

Tong, Y.-B., Yang, Z., Zheng, L.-D., Xu, Y.-L., Wang, H., Gao, L., & Hu, X.-Z. (2013). Internal crustal deformation in the northern part of Shan-Thai Block: New evidence from paleomagnetic results of Cretaceous and Paleogene redbeds. *Tectonophysics*, *608*, 1138–1158. doi: 10.1016/j.tecto.2013.06.031

Torsvik, T. H., Van der Voo, R., Preeden, U., Mac Niocaill, C., Steinberger, B., Doubrovine, P. V., ... Cocks, L. R. M. (2012). Phanerozoic polar wander, palaeogeography and dynamics. *Earth-Science Reviews*, *114*(3), 325–368. doi: 10.1016/j.earscirev.2012.06.007

Vaes, B., Li, S., Langereis, C. G., & van Hinsbergen, D. J. J. (2021). Reliability of palaeomagnetic poles from sedimentary rocks. *Geophysical Journal International*, *225*(2), 1281–1303. doi: 10.1093/gji/ggab016

van Hinsbergen, D. J., Krijgsman, W., Langereis, C. G., Cornée, J.-J., Duermeijer, C. E., & van Vugt, N. (2007). Discrete Plio-Pleistocene phases of tilting and counterclockwise rotation in the southeastern Aegean arc (Rhodos, Greece): early Pliocene formation of the south Aegean left-lateral strike-slip system. *Journal of the Geological Society*, *164*(6), 1133–1144. doi: 10.1144/0016-76492006-061

van Hinsbergen, D. J. J., Dekkers, M. J., & Koc, A. (2010). Testing Miocene remagnetization of Bey Dağları: Timing and amount of Neogene rotations in SW Turkey. *Turkish Journal of Earth Sciences*, *19*(2), 123–156.

van Hinsbergen, D. J. J., Lippert, P. C., Dupont-Nivet, G., McQuarrie, N., Doubrovine, P. V., Spakman, W., & Torsvik, T. H. (2012). Greater India Basin hypothesis and a two-stage Cenozoic collision between India and Asia. *Proceedings of the National Academy of Sciences*, *109*(20), 7659–7664. doi: 10.1073/pnas.1117262109

van Toorenenburg, K. A., Donselaar, M. E., & Weltje, G. J. (2018). The life cycle of crevasse splays as a key mechanism in the aggradation of alluvial ridges and river avulsion. *Earth Surface Processes and Landforms*, *43*(11), 2409–2420. doi: 10.1002/esp.4404

Vaughn, J., Kodama, K. P., & Smith, D. P. (2005). Correction of inclination shallowing and its tectonic implications: The Cretaceous Perforada Formation, Baja California. *Earth and Planetary Science Letters*, *232*(1-2), 71–82. doi: 10.1016/j.epsl.2004.11.026

Westerweel, J., Roperch, P., Licht, A., Dupont-Nivet, G., Win, Z., Poblete, F., ... Aung, D. W. (2019). Burma Terrane part of the Trans-Tethyan arc during collision with India according to palaeomagnetic data. *Nature Geoscience*, *12*(10), 863–868. doi: 10.1038/s41561-019-0443-2

Yan, M., Van der Voo, R., Tauxe, L., Fang, X., & M Parés, J. (2005). Shallow bias in Neogene palaeomagnetic directions from the Guide Basin, NE Tibet, caused by inclination error. *Geophysical Journal International*, *163*(3), 944–948. doi: 10.1111/j.1365-246X.2005.02802.x

Zhang, Y., Huang, W., Huang, B., Hinsbergen, D. J. J., Yang, T., Dupont-Nivet, G., & Guo, Z. (2018). 53–43 Ma deformation of eastern Tibet revealed by three stages of tectonic rotation in the Gongjue Basin. *Journal of Geophysical Research: Solid Earth*, *123*(5), 3320–3338. doi: 10.1002/2018jb015443

Zhang, Y., Swanson-Hysell, N. L., Schmitz, M. D., Miller, J. D., & Avery, M. S. (2021). Synchronous emplacement of the anorthosite xenolith-bearing Beaver River diabase and one of the largest lava flows on Earth. *Geochemistry, Geophysics, Geosystems*, *22*(10), e2021GC009909. doi: 10.1029/2021GC009909

Özdemir, , & Dunlop, D. J. (2014). Hysteresis and coercivity of hematite. *Journal of Geophysical Research: Solid Earth*, *119*(4), 2582–2594. doi: 10.1002/2013JB010739

Supporting Information for "Quantifying inclination shallowing and representing flattening uncertainty in sedimentary paleomagnetic poles"

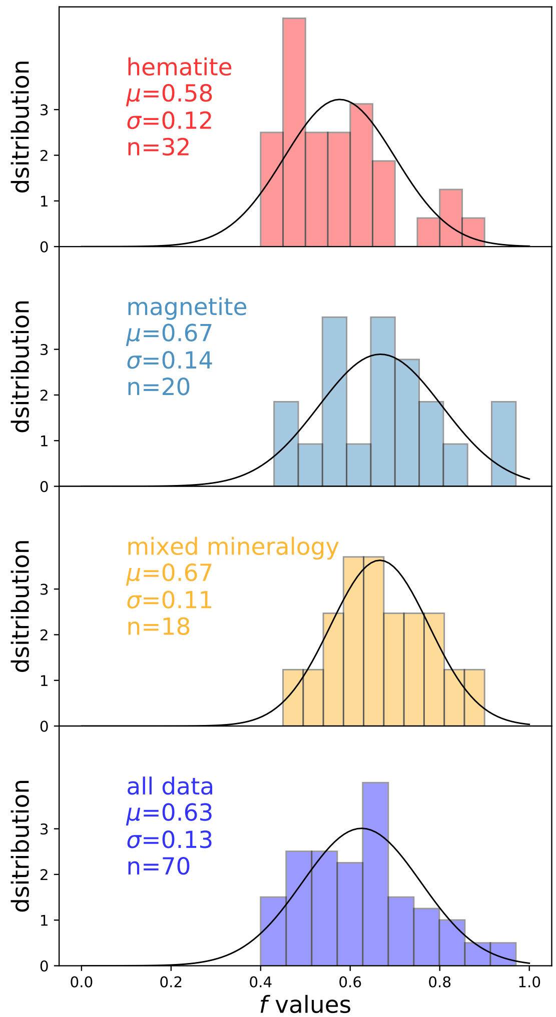

Figure S1. Distribution of f factors building on the compilations of Bilardello (2016) and Vaes et al. (2021), we compiled f factors from both anisotropy and E/I methods from clastic sedimentary rocks (Table S1). The distributions of f factors are categorized by remanence carrying mineralogy (hematite, magnetite, or a mix of hematite and magnetite). Also shown is the distribution of all compiled f values. For each category, we fit the data with a normal distribution (black curves) and report the mean and one standard devation values such that one can use these values in the *ipmag.find_compilation_kent* function in the Python package PmagPy Tauxe et al. (2016) to estimate uncertainties associated with a Kent distribution for legacy paleomagnetic data.

Table S1. Compilation of published f factors

locality	lithology	f	f_min	f_max	ref	mineralogy	method	n
Subei	red beds	0.49	0.37	0.64	Tauxe and Kent, 2004	hematite	EI	222
Potwar	red beds	0.77	0.58	1.11	Tauxe, 2005	hematite	EI	105
Gudie	fluvial sediments	0.63	0.47	0.73	Yan et al., 2005	mixed	EI	627
Dan River	red siltstone and gray/black mud	0.59	0.49	0.74	Kent and Tauxe, 2005	mixed	EI	333
Princeton	red beds	0.57	0.39	1.04	Kent and Tauxe, 2005	hematite	EI	148
Nursery	red beds	0.4	0.33	0.54	Kent and Tauxe, 2005	hematite	EI	194
Titusville	red beds	0.63	0.54	0.76	Kent and Tauxe, 2005	hematite	EI	308
Rutgers	red beds	0.66	0.57	0.73	Kent and Tauxe, 2005	hematite	EI	336
Somerset	red beds	0.63	0.53	0.73	Kent and Tauxe, 2005	hematite	EI	309
Weston	red beds	0.49	0.42	0.59	Kent and Tauxe, 2005	hematite	EI	246
Martinsville	red beds	0.49	0.42	0.59	Kent and Tauxe, 2005	hematite	EI	302
Jameson Land	red beds	0.58	0.47	0.81	Kent and Tauxe, 2005	hematite	EI	222
Hartford	red beds	0.54	0.48	0.62	Kent and Olson, 2008	hematite	EI	315
Calatayud basin	fluvial and lacustrine sediments	0.73	0.63	0.84	Krijgsman and Tauxe, 2004	mixed	EI	648
Nanaimo	marine mud- and siltstones	0.97	0.79	1.05	Krijgsman and Tauxe, 2006	magnetite	EI	143
Kefala & Aspropetres	palustrine and lacustrine sediments	0.59	0.37	0.89	Van Hinsbergen et al., 2007	magnetite	EI	75
Nacimiento	claystones and siltstones	0.84	0.5	1.01	Tauxe et al., 2008	hematite	EI	102
Dome de Barrot	red mudstone and purple siltstone	0.9	0.79	1.03	Haldan et al., 2009	hematite	EI	411
Lodeve (Kungurian Äï Wordian)	red siltstones and calcareous siltstone	0.78	0.37	1	Haldan et al., 2009	mixed	EI	146
Lodeve (Sakmarian-Artinskian)	red siltstones and calcareous siltstone	0.83	0.63	1.16	Haldan et al., 2009	mixed	EI	143
Artes	red beds	0.58	0.42	0.77	Costa et al., 2009	mixed	EI	221
TA5	turbiditic volcanoclastics	0.94	0.68	1	Meijers et al., 2010	magnetite	EI	115
CtgÄêXsh	red beds	0.78	0.51	1	Dupont-Nivet et al., 2010	mixed	EI	95
Xiejia	red beds	0.9	0.72	1.04	Dupont-Nivet et al., 2010	mixed	EI	185
Mahalagou	red beds	0.68	0.54	0.78	Dupont-Nivet et al., 2010	mixed	EI	228
Shexing	red beds	0.48	0.44	0.52	Tan et al., 2010	hematite	EI	377
Korkuteli	blue clays and turbiditic sandstone	0.67	0.53	0.83	Van Hinsbergen et al., 2010	mixed	EI	192
Shexing	red beds	0.66	0.53	0.91	Van Hinsbergen et al., 2012	hematite	EI	100
Karoo basin	fluvial sand-, silt- and mudstone	0.7	0.41	0.9	Lanci et al., 2013	magnetite	EI	136
Linzizong	volcaniclastics and mudstones	0.43	0.32	0.57	Hunag et al., 2013	magnetite	EI	119
Mengla	red beds	0.45	0.38	0.55	Tong et al., 2013	mixed	EI	85
Sonkul Basin (DUN)	red beds	0.58	0.44	0.8	Kirsher et al, 2014	hematite	EI	115
Sonkul Basin (DUN)	red beds	0.58	0.44	0.8	Kirsher et al, 2014	magnetite	EI	115
Kangtuo lower section	red beds	0.53	0.46	0.6	Ding et al., 2015	hematite	EI	414
Kangtuo upper section	red beds	0.42	0.33	0.56	Ding et al., 2015	hematite	EI	137
Sangsang	turbiditic sandstones	0.51	0.4	0.66	Hunag et al., 2015	magnetite	EI	117

Table S1. Compilation of published f factors

locality	lithology	f	f_min	f_max	ref	mineralogy	method	n
Qushenla	red beds	0.61	0.49	0.76	Chen et al, 2017	mixed	EI	174
Sangsang	red beds	0.52	0.42	0.72	Meng et al., 2017	mixed	EI	223
Gonjo NE limb	red beds	0.62	0.52	0.78	Tong et al., 2017	mixed	EI	102
Gonjo SW limb	red beds	0.73	0.58	0.94	Tong et al., 2017	mixed	EI	203
Gongjue	red beds	0.66	0.54	0.81	Zhang et al., 2018	mixed	EI	150
Ranmugou	red beds	0.55	0.47	0.64	Zhang et al., 2018	mixed	EI	178
Rehbrein Creek	shales and quart-rich turbidites	0.47	0.37	0.61	Dallanave et al., 2018	magnetite	EI	133
Lainbach Valley	claystone and calcarenites	0.77	0.59	0.98	Dallanave et al., 2018	magnetite	EI	87
Yaw	mudstones, sandstones and siderite beds	0.62	0.4	1.29	Westerweel et al., 2019	magnetite	EI	168
NW James Ross Island	sandstones and mudstones	0.54			Milanese et al., 2019	magnetite	EI	119
Gonjo 1	red beds	0.46	0.32	0.68	Vaes et al., 2021	hematite	EI	128
Gonjo 2	red beds	0.56	0.43	0.8	Vaes et al., 2021	hematite	EI	145
Gonjo 3	red beds	0.64	0.48	0.84	Vaes et al., 2021	hematite	EI	129
Gonjo 4	red beds	0.47	0.35	0.64	Vaes et al., 2021	hematite	EI	137
Gonjo 5	red beds	0.48	0.33	0.69	Vaes et al., 2021	hematite	EI	156
Gonjo 6	red beds	0.44	0.31	0.62	Vaes et al., 2021	hematite	EI	133
Gonjo 8	red beds	0.52	0.41	0.7	Vaes et al., 2021	hematite	EI	167
Gonjo 9	red beds	0.65	0.51	0.84	Vaes et al., 2021	hematite	EI	167
Qubeiya and Jialazi Fms	sandstone, siltstone, wackestone	0.81	0.62	0.99	Li et al., 2022	magnetite	EI	87
Cut Face	red beds	0.64	0.5	0.86	Pierce et al., 2022	hematite	EI	157
Pigeon Point	mud- silt- and sandstone	0.71			Kodama and Davi, 1995	magnetite	anisotropy	
Nacimiento	claystones and shaless and siltstones and sandstones	0.79			Kodama, 1997	magnetite	anisotropy	
Ladd	claystones and shaless and siltstones and sandstones	0.65			Tan and Kodama, 1998	magnetite	anisotropy	
Point Loma	claystones and shaless and siltstones and sandstones	0.56			Tan and Kodama, 1998	magnetite	anisotropy	
Valle	sandstone	0.69			Li et al., 2001	magnetite	anisotropy	
Kapusaliang	red beds	0.43			Tan et al., 2003	hematite	anisotropy	
Nanaimo	marine mud- and sandstones	0.7			Kim and Kodama, 2004	magnetite	anisotropy	
Perforada	interbedded mudstone and sandstone	0.67			Vaughn et al., 2005	magnetite	anisotropy	
Glenshaw	limestone and siltstone	0.65			Kodama, 2009	magnetite	anisotropy	
Mauch Chunk	calcareous mudstone and sandstone	0.49			Bilardello and Kodama 2010a	hematite	anisotropy	
Deer Lake	red beds	0.54			Bilardello and Kodama 2010b	hematite	anisotropy	
Shepody	red beds	0.64			Bilardello and Kodama, 2010c	hematite	anisotropy	
Maringouin	red beds	0.83			Bilardello and Kodama, 2010c	hematite	anisotropy	
Itarare	marine rhythmites and diamictites and shale and sandstones	0.68			Bilardello et al. 2018	mixed	anisotropy	

References

Bilardello, D., 2016, The do's and don'ts of inclination shallowing corrections: The IRM Quarterly, vol. 26, p. 12.

Tauxe, L., Shaar, R., Jonestrask, L., Swanson-Hysell, N. L., Minnett, R., Koppers, A. a. P., Constable, C. G., Jarboe, N., Gaastra, K., and Fairchild, L., 2016, PmagPy: Software package for paleomagnetic data analysis and a bridge to the Magnetics Information Consortium (MagIC) Database: Geochemistry, Geophysics, Geosystems, vol. 17, pp. 2450–2463, doi:10.1002/2016GC006307.

Vaes, B., Li, S., Langereis, C. G., and van Hinsbergen, D. J. J., 2021, Reliability of palaeomagnetic poles from sedimentary rocks: Geophysical Journal International, vol. 225, pp. 1281–1303, doi:10.1093/gji/ggab016.